Metalloprotease-Dependent Attenuation of BMP Signaling Restricts Cardiac Neural Crest Cell Fate

AUTHOR(S):

Arai, Hiroyuki N.; Sato, Fuminori; Yamamoto, Takuya; Woltjen, Knut; Kiyonari, Hiroshi; Yoshimoto, Yuki; Shukunami, Chisa; Akiyama, Haruhiko; Kist, Ralf; Sehara-Fujisawa, Atsuko

CITATION:

Arai, Hiroyuki N. ...[et al]. Metalloprotease-Dependent Attenuation of BMP Signaling Restricts Cardiac Neural Crest Cell Fate. Cell Reports 2019, 29(3): 603-616.e5

ISSUE DATE:

2019-10-15

URL:

http://hdl.handle.net/2433/244338

Article

Cell Reports

Metalloprotease-Dependent Attenuation of BMP Signaling Restricts Cardiac Neural Crest Cell Fate

Graphical Abstract

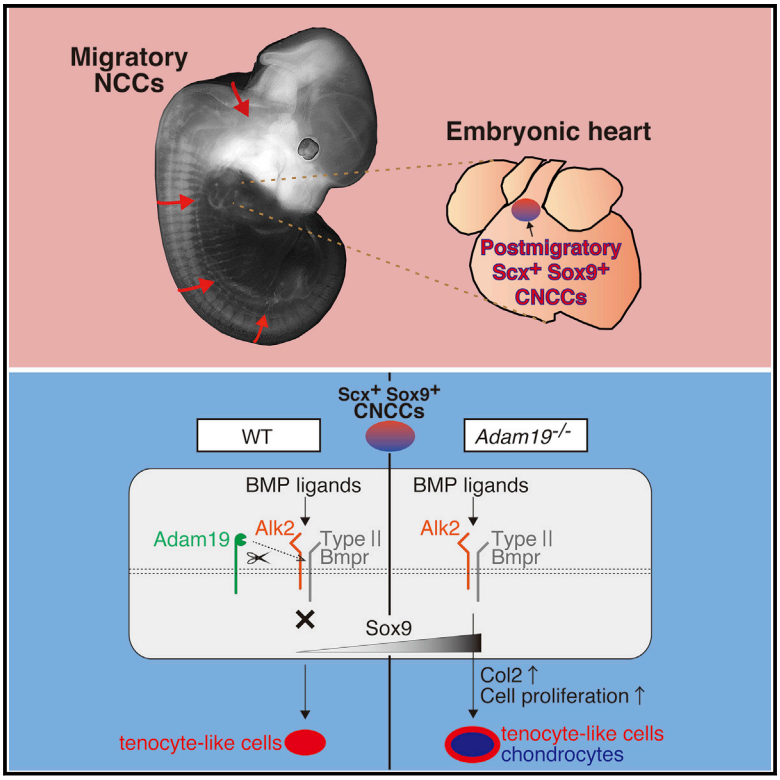

Highlights

- *Adam19* mutants exhibit neural crest-derived cardiac cartilage formation
- High Sox9 expression in *Adam19*$^{-/-}$-CNCCs induces cardiac cartilage formation
- Adam19 mediates proteolytic cleavage of BMP receptor Alk2
- Adam19 suppresses CNCC chondrogenesis by inhibiting the BMP-Sox9 signaling pathway

Authors

Hiroyuki N. Arai, Fuminori Sato, Takuya Yamamoto, ..., Haruhiko Akiyama, Ralf Kist, Atsuko Sehara-Fujisawa

Correspondence

arai.hiroyuki.6e@kyoto-u.ac.jp (H.N.A.), sehara.atsuko.3m@kyoto-u.ac.jp (A.S.-F.)

In Brief

Arai et al. show that metalloprotease Adam19 is essential for proper differentiation of cardiac neural crest cells (CNCCs) in murine embryogenesis. Adam19 suppresses the response of CNCCs to bone morphogenic protein by cleaving its receptor Alk2, thus restricting CNCC skeletogenic potential and preventing cartilage formation in the heart.

Arai et al., 2019, Cell Reports *29*, 603–616
October 15, 2019
https://doi.org/10.1016/j.celrep.2019.09.019

CellPress

Cell Reports
Article

Metalloprotease-Dependent Attenuation of BMP Signaling Restricts Cardiac Neural Crest Cell Fate

Hiroyuki N. Arai,[1,*] Fuminori Sato,[1] Takuya Yamamoto,[2,3,4,5] Knut Woltjen,[2,6] Hiroshi Kiyonari,[7] Yuki Yoshimoto,[8,12] Chisa Shukunami,[8] Haruhiko Akiyama,[9] Ralf Kist,[10,11] and Atsuko Sehara-Fujisawa[1,13,*]

[1]Department of Regeneration Science and Engineering, Institute for Frontier Life and Medical Sciences, Kyoto University, Kyoto 606-8507, Japan
[2]Department of Life Science Frontiers, Center for iPS Cell Research and Application (CiRA), Kyoto University, Kyoto 606-8507, Japan
[3]Institute for the Advanced Study of Human Biology (WPI-ASHBi), Kyoto University, Yoshida-Konoe-cho, Sakyo-ku, Kyoto 606-8501 Japan
[4]AMED-CREST, AMED 1-7-1 Otemachi, Chiyodaku, Tokyo 100-0004, Japan
[5]Medical Risk Avoidance Based on iPS Cells Team, RIKEN Center for Advanced Intelligence Project (AIP), Kyoto 606-8507, Japan
[6]Hakubi Center for Advanced Research, Kyoto University, Kyoto 606-8501, Japan
[7]Laboratory for Animal Resources and Genetic Engineering, RIKEN Center for Biosystems Dynamics Research, Kobe 650-0047, Japan
[8]Department of Molecular Biology and Biochemistry, Division of Dental Sciences, Biomedical Sciences Major, Graduate School of Biomedical and Health Sciences, Hiroshima University, Hiroshima 734-8553, Japan
[9]Department of Orthopedic Surgery, Gifu University Graduate School of Medicine, Gifu 501-1194, Japan
[10]Centre for Oral Health Research, School of Dental Sciences, Newcastle University, Newcastle upon Tyne NE2 4BW, UK
[11]Institute of Genetic Medicine, International Centre for Life, Newcastle University, Newcastle upon Tyne NE1 3BZ, UK
[12]Present address: Muscle Aging and Regenerative Medicine, Research Team for Geriatric Medicine, Tokyo Metropolitan Institute of Gerontology, 35-2 Sakae-cho, Itabashi, Tokyo 173-0015, Japan
[13]Lead Contact
*Correspondence: arai.hiroyuki.6e@kyoto-u.ac.jp (H.N.A.), sehara.atsuko.3m@kyoto-u.ac.jp (A.S.-F.)
https://doi.org/10.1016/j.celrep.2019.09.019

SUMMARY

In higher vertebrates, cephalic neural crest cells (NCCs) form craniofacial skeleton by differentiating into chondrocytes and osteoblasts. A subpopulation of cephalic NCCs, cardiac NCCs (CNCCs), migrates to the heart. However, CNCCs mostly do not yield skeletogenic derivatives, and the molecular mechanisms of this fate restriction remain elusive. We identify a disintegrin and metalloprotease 19 (Adam19) as a position-specific fate regulator of NCCs. Adam19-depleted mice abnormally form NCC-derived cartilage in their hearts through the upregulation of Sox9 levels in CNCCs. Moreover, NCC-lineage-specific *Sox9*-overexpressing mice recapitulate CNCC chondrogenesis. *In vitro* experiments show that Adam19 mediates the cleavage of bone morphogenic protein (BMP) type I receptor Alk2 (Acvr1), whereas pharmacogenetic approaches reveal that Adam19 inhibits CNCC chondrogenesis by suppressing the BMP-Sox9 cascade, presumably through processing Alk2. These findings suggest a metalloprotease-dependent mechanism attenuating cellular responsiveness to BMP ligands, which is essential for both the positional restriction of NCC skeletogenesis and normal heart development.

INTRODUCTION

Neural crest cells (NCCs) possess a unique ability to generate morphologically and functionally different cell types, including neurons, smooth muscle cells, melanocytes, and chondrocytes. During vertebrate development, NCCs initially arise from the dorsal neural tube as multipotent stem/progenitor cells and, owing to their migratory properties, move readily within embryonic tissues (Le Douarin and Kalcheim, 1999). NCCs contribute to the development of most organs in the body, which raises an intriguing question of position-specific fate restriction in multipotent NCCs during embryogenesis. The cephalic domain of the neural crest yields NCCs differentiating into skeletogenic chondrocytes and osteoblasts only in the head and neck regions, whereas in other body parts, bones and cartilages are of mesodermal origin (Dupin et al., 2018). It has been suggested that the differential expression of *Hox* genes along the anteroposterior axis limits the ability of NCC skeletogenesis (Le Douarin et al., 2004). Thus, dermal bones are derived only from Hox^- NCCs, whereas transfection with the *Hox* genes can abolish the skeletogenic ability of cranial NCCs (Le Douarin et al., 2004; Abzhanov et al., 2003; Creuzet et al., 2002). It is unclear, however, whether there is a mechanism that limits the NCC skeletogenesis in the heart located between the head and trunk regions.

Cardiac NCCs (CNCCs) are a subpopulation of cephalic NCCs that migrate into the heart; they derive from a Hox^+ region (rhombomere levels 6–8) posterior to the area where *Hox*-dependent regulations are observed (rhombomere level 4) (Etchevers et al., 2001; Minoux et al., 2009). Transcription factor *Ets1* or extracellular matrix protein *fibronectin 1* (*Fn1*) mutant mice exhibit NCC-derived cartilage formation in their hearts (Chen et al., 2015; Gao et al., 2010), implying that CNCCs have yet-unknown programs restricting skeletogenesis other than *Hox* genes. Abnormal cardiac chondrogenesis can be observed in humans with heart disease of unexplained etiology, such as sudden infant death syndrome (Ferris and Aherne, 1971), suggesting that certain pathological conditions in the heart may be related to

the deficiency in the mechanisms limiting CNCC skeletogenic differentiation.

CNCCs play a crucial role in heart development, including remodeling of pharyngeal arches, aorticopulmonary septation, and valvulogenesis. Consequently, defects in CNCC differentiation are associated with human cardiocraniofacial diseases such as DiGeorge, velocardiofacial, and coloboma, heart defects, atresia choanae, growth retardation, genital abnormalities, and ear abnormalities (CHARGE) syndromes (Kirby et al., 1983; Keyte and Hutson 2012). Therefore, understanding fundamental molecular pathways controlling CNCC differentiation is important for lowering the risk of congenital heart defects. However, mechanisms controlling CNCC fate in the aorticopulmonary (AP) septum are unknown.

A transmembrane protein, Adam19 (a disintegrin and metalloprotease), is suggested as one of the candidate regulatory factors in CNCC fate determination, because Adam19 knockout mice show membranous ventricular septal defects similar to those caused by *Ets1* or *Fn1* defects (Chen et al., 2015; Gao et al., 2010; Kurohara et al., 2004; Zhou et al., 2004). Moreover, Adam19 expression in NCCs is required for the formation of the ventricular septum and valves in the heart (Komatsu et al., 2007). Despite these facts, the physiological and molecular mechanisms underlying the contribution of Adam19 to heart development are poorly understood.

ADAM proteases mediate ectodomain shedding of transmembrane proteins such as membrane-anchored growth factors and play crucial roles in development (Weber and Saftig, 2012). Adam19 has a proteolytic-active extracellular domain (Chesneau et al., 2003; Shirakabe et al., 2001) and has been reported to participate in the proteolytic processing of cadherin-6B in chick premigratory cranial NCCs (Schiffmacher et al., 2014); it can also perform a nonproteolytic function by stabilizing Adam13, which induces the expression of NCC markers in *Xenopus* (Li et al., 2018). However, the substrate of Adam19 in mammalian heart development has not been identified.

In this study, we explored the molecular characteristics of CNCCs related to their phenotypic commitment in the heart and identified Adam19 as a positional gatekeeper that is critical for defining appropriate CNCC fate in development. In mice lacking *Adam19*, CNCCs differentiated into chondrocytes and formed abnormal cartilage in the heart through the upregulation of Sox9 levels. Adam19 mediated the ectodomain shedding of bone morphogenic protein (BMP) receptor Alk2 and inhibited the BMP-Sox9 cascade in the heart. Our study presents a cell-autonomous mechanism of CNCC fate limitation based on Adam19-mediated suppression of BMP signaling in the developing heart.

RESULTS

Preferential Expression of Adam19 in Cardiac NCCs and Abnormal Cartilage Formation in *Adam19*$^{-/-}$ Hearts

To visualize NCC-lineage cells in the mouse, we crossed *Wnt1-Cre* mice with *Rosa26*$^{CAG\text{-}LSL\text{-}tdTomato/+}$ (*R26*^{tdT}) mice and obtained the *Wnt1-Cre;R26*^{tdT} mouse line (Danielian et al., 1998; Madisen et al., 2010), in which NCCs were genetically labeled by a fluorescent protein tdTomato (tdT). To measure *Adam19* mRNA levels in postmigratory CNCCs, we performed qPCR on tdT^{+} NCC populations that were isolated from dissected parts of *Wnt1-Cre;R26*^{tdT} mouse embryos (Figure 1A, tpo panel) using fluorescence-activated cell sorting (FACS). The results showed that CNCCs exhibited significantly higher *Adam19* expression compared with cranial and trunk NCC populations and non-neural crest-derived heart cells at embryonic day (E) 13.5 (Figure 1A, bottom panel). After migration, CNCCs were condensed in the AP septum and were surrounded by myosin heavy chain 1^{+} (Myh1^{+}) myocardium (Figure 1B). To assess the pattern of *Adam19*-expressing cells, we generated *Adam19*$^{Venus/+}$ knockin mice by inserting the *Venus* gene encoding an improved-type GFP derivative into the *Adam19* genomic locus (Figures S1A–S1C). Consistent with qPCR results, *Adam19*-Venus fluorescence was preferentially observed in the heart of *Adam19*$^{Venus/+}$ mice at E13.5 (Figures S1D and S1E). Similar to the localization pattern of tdT^{+} CNCCs in *Wnt1-Cre;R26*^{tdT} mouse hearts (Figure 1B), *Adam19*-Venus was detected in the aorta and pulmonary trunk at E13.5 (Figure 1C), in the developing AP septum around E12.5–E16.5, and in cardiac endothelial cells during all of the analyzed embryonic stages (E10.5–E18.5), but was hardly seen around aortic arch arteries where migrating CNCCs were already located at E10.5 (Figure S2A). These results revealed that postmigratory CNCCs in the AP septum expressed Adam19.

In the postmigratory CNCCs, Adam19 protein was detected near the cell surface (Figure S2B, yellow arrowheads) and around the cell nuclei (Figure S2B, white arrowheads), which is consistent with the location of the Golgi apparatus (Yokozeki et al., 2007).

Analysis of Alcian blue-stained whole-mount embryonic hearts revealed the formation of a nodule between the aorta and pulmonary artery (the AP septum region) in perinatal *Adam19*$^{-/-}$ mice, which displayed cartilaginous structure (Figure 1D). Although Alcian blue-stained nodules were also observed in one wild-type (WT) heart (1/10) and some *Adam19*$^{+/-}$ hearts (4/10), they were found in all of the *Adam19*$^{-/-}$ hearts (10/10), in which they were significantly larger than those in WT or *Adam19*$^{+/-}$ embryos (Figure 1E) and were detectable from E15.5 onward, but not at E14.5 (Figure S2C). Immunostaining for Sox9, a transcription factor of the chondrogenic lineage, and cartilage extracellular matrix proteins aggrecan (Acan) and type II collagen (Col2) confirmed the presence of cartilage nodules in *Adam19*$^{-/-}$ hearts but not in WT hearts at E18.5 (Figure S2D). Thus, *Adam19*$^{-/-}$ hearts developed histologically and molecularly defined cartilages.

The Abnormal Cartilage Is Derived from CNCCs Typically Differentiating into Tenocyte-like Cells

To investigate whether the ectopic cartilage in *Adam19*$^{-/-}$ hearts had the CNCC origin, we performed genetic lineage tracing analysis. Given that endocardial cushion mesenchyme comprises two cell types derived from endothelial cells and NCCs (Jiang et al., 2000; Kovacic et al., 2012), we crossed *Tie2-Cre* (endothelial cell origin) (Kisanuki et al., 2001) or *Wnt1-Cre* (neural crest cell origin) mice with *R26*^{tdT} reporter mice to visualize each cell lineage. As expected, in the cartilage of *Adam19*$^{-/-}$*;Tie2-Cre;R26*^{tdT} hearts, there were no tdT^{+} cells, whereas in the cartilage of *Adam19*$^{-/-}$*;Wnt1-Cre; R26*^{tdT} hearts,

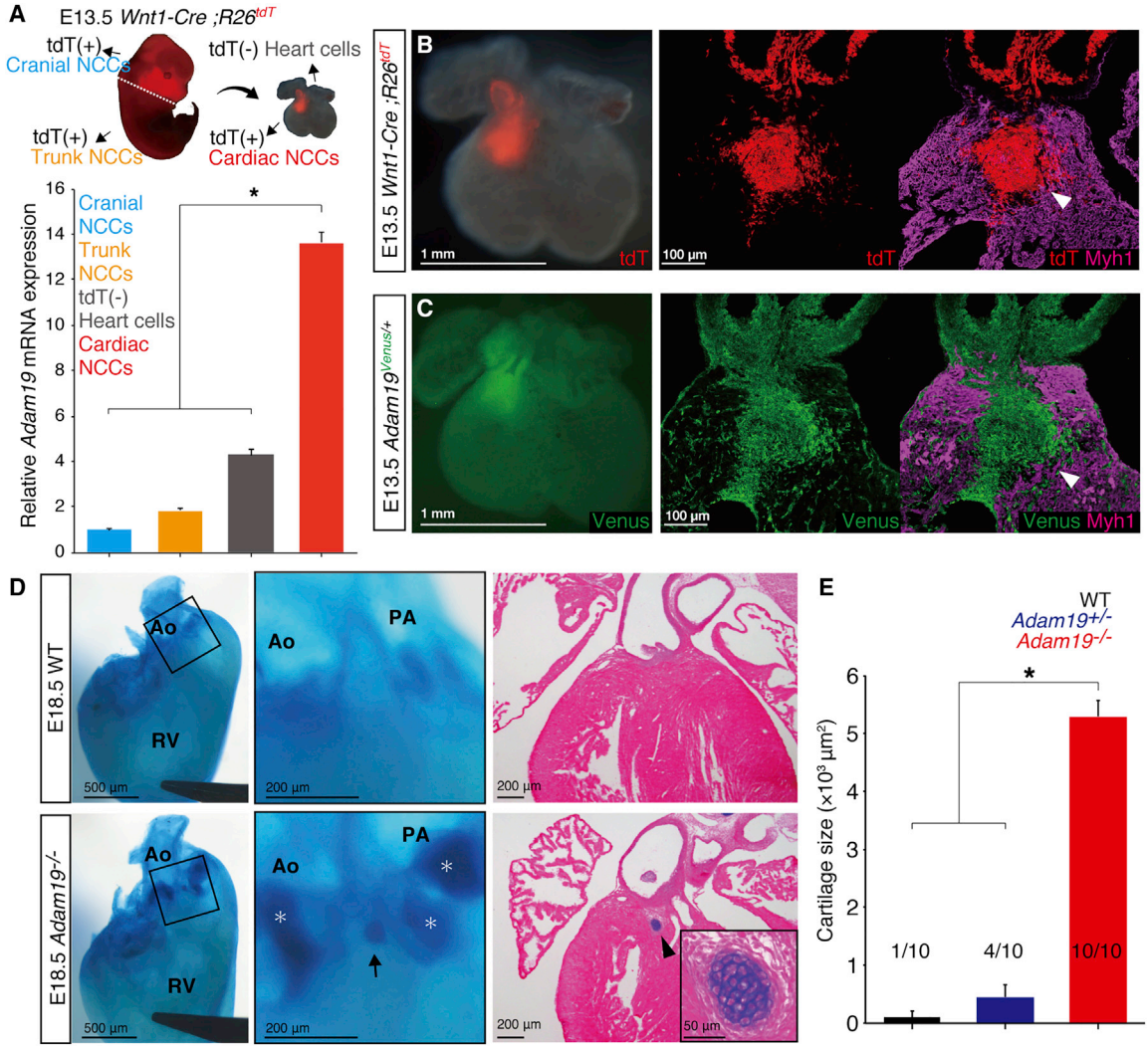

Figure 1. Preferential Expression of Adam19 in Cardiac NCCs and Abnormal Cartilage Formation in *Adam19*$^{-/-}$ Hearts

(A) *Adam19* mRNA expression in FACS-sorted cell populations was assessed by qPCR (n = 3 embryos). The level of *Adam19* mRNA in cranial NCCs was defined as 1.

(B) *Wnt1-Cre;R26*^{tdT} heart at E13.5. Overall view (left panel). A heart section labeled with tdT (NCC lineage) and immunostained for myosin heavy chain 1 (Myh1; right panel).

(C) *Adam19*$^{Venus/+}$ heart at E13.5. Overall view (left panel). A heart section immunostained for Venus (anti-GFP antibody) and Myh1 (right panel). Arrowheads indicate the AP septum. See also Figures S1, S2A, and S2B.

(D) Hearts of WT and *Adam19*$^{-/-}$ mice at E18.5. Right lateral views of Alcian blue-stained hearts (left panels). High-magnification images of boxed areas (center panels). Eosin- and Alcian blue-stained heart sections (right panels). The inset shows a magnified view of the cartilage. Asterisks indicate hyperplastic valves in *Adam19*$^{-/-}$ mice and arrows indicate ectopic cartilages. Ao, aorta; PA, pulmonary artery; RV, right ventricle.

(E) Sizes of cartilaginous nodules calculated as maximal Alcian blue^{+} areas in WT, *Adam19*$^{+/-}$, and *Adam19*$^{-/-}$ hearts at E18.5 (n = 10 embryos). The data are shown as means ± SEMs; *p < 0.05. See also Figures S2C and S2D.

all of the cells were tdT^{+} and located at the center of the CNCC cluster (Figure 2A), indicating that the abnormal cartilage was derived from CNCCs. Similar but smaller CNCC clusters were also observed in *Adam19*$^{+/+}$*;Wnt1-Cre;R26*^{tdT} hearts at the same position as in *Adam19*$^{-/-}$ hearts (Figure 2A). A three-dimensional reconstruction of whole-mount immunostaining revealed a bridge-like structure of CNCC clusters between the aorta and pulmonary artery and showed the presence of Col2^{+} cartilage in *Adam19*$^{-/-}$-CNCC but not in *Adam19*$^{+/+}$-CNCC clusters (Figure 2B; Video S1). These observations raised a question regarding the terminal differentiation characteristics of CNCC clusters in WT mice.

CNCCs migrating into the heart separate the common outflow tract into the aortic and pulmonary trunks, and some of them differentiate into smooth muscle cells surrounding the aorta and pulmonary arteries (Jiang et al., 2000; Waldo et al., 1998). However, little is known about the fate of the CNCC subpopulation that reaches the AP septum. CNCCs

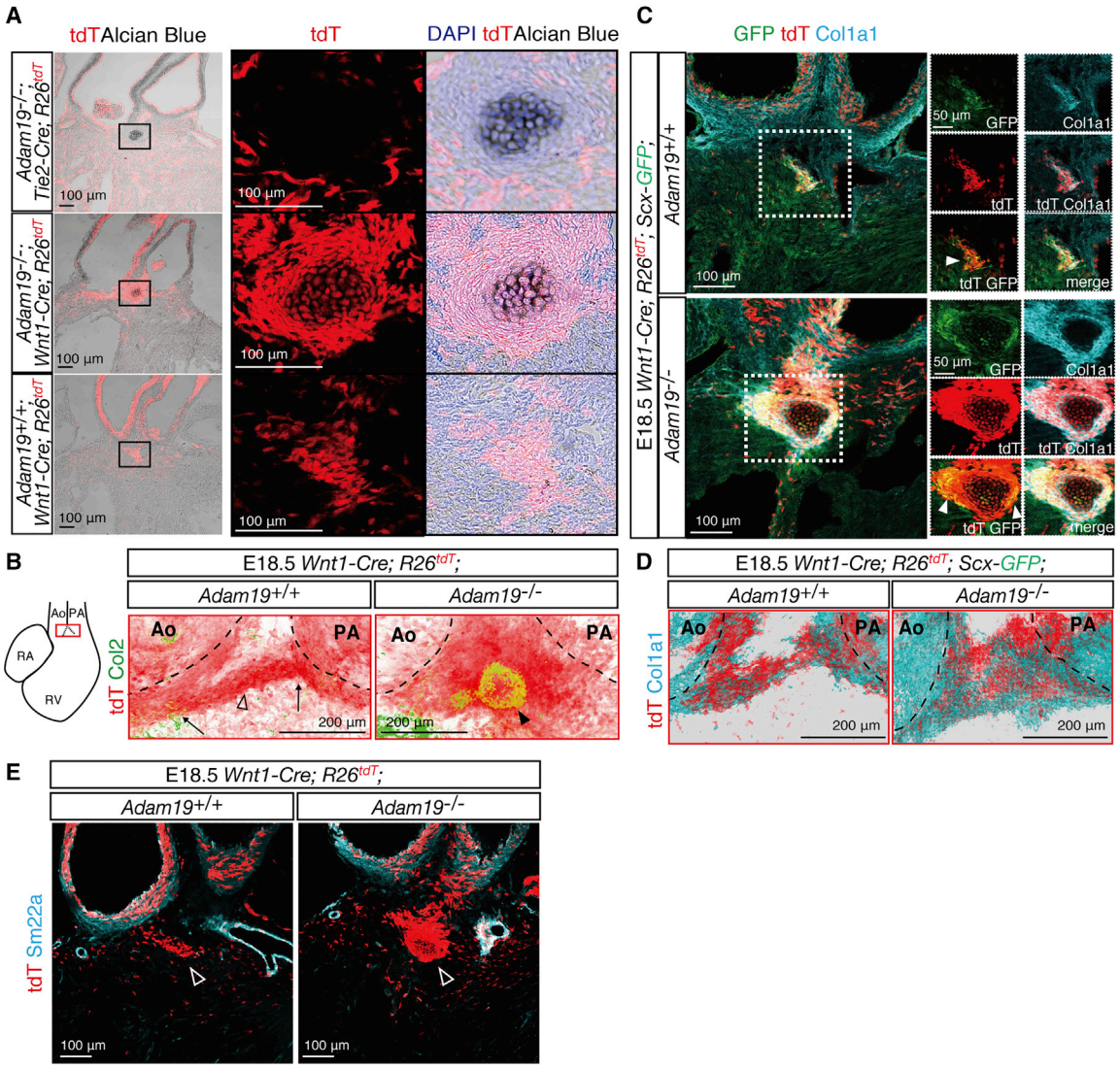

Figure 2. Abnormal Cartilage in *Adam19*$^{-/-}$ Hearts Is Formed by CNCCs Typically Differentiating into Tenocyte-like Cells

(A) DAPI- and Alcian blue-stained heart sections at E18.5 (left panels) with magnified images of the boxed areas (center and right panels).

(B) Schematic representation of the heart; the observed area is indicated by a red box (left). Three-dimensional reconstruction of whole-mount hearts immunostained for Col2 showing the absence (*Adam19*$^{+/+}$; open arrowhead) or presence (*Adam19*$^{-/-}$; closed arrowhead) of Col2^{+} structures (right panels). Arrows indicate the connection between the aorta and pulmonary artery. Ao, aorta; PA, pulmonary artery; RA, right atrium; RV, right ventricle. See also Video S1.

(C) Sections of *Adam19*$^{+/+}$*;Scx-GFP* and *Adam19*$^{-/-}$*;Scx-GFP* hearts (E18.5) immunostained for Col1a1 and Scx-GFP. Arrowheads indicate Scx^{+} CNCCs.

(D) Three-dimensional reconstruction of whole-mount hearts immunostained for Col1a1. See also Video S2.

(E) Sections immunostained for smooth muscle cell marker Sm22a. Open arrowheads indicate Sm22a^{-} CNCC clusters.

in the AP septum are adjacent to semilunar valves (Waldo et al., 1998); therefore, we hypothesized that CNCC clusters had the same characteristics as cardiac valvular cells, which are similar in their genetic profile to tenocytes or ligament cells and express transcription factor scleraxis (Scx) and extracellular matrix protein type I collagen (Col1a1) (Levay et al., 2008; Murchison et al., 2007). To examine the expression of tenogenic marker Scx in CNCCs of the AP septum, we used *Scx*-GFP transgenic mice (Sugimoto et al., 2013a). Analysis of *Scx-GFP;Wnt1-Cre;R26*^{tdT} hearts at E18.5 revealed that CNCCs in the clusters expressed tenocyte markers Scx (Murchison et al., 2007) and Col1a1 (Figures 2C and 2D; Video S2) but not the smooth muscle cell marker Sm22a (Figure 2E), indicating that WT CNCCs in the AP septum differentiated into the tenogenic lineage.

Adam19 Expression in CNCCs Is Required for Their Proper Cell Fate Decision

To determine which Adam19-expressing cell types were required for proper CNCC differentiation, we generated mice with a conditional *Adam19*-knockout allele (*Adam19*$^{fl/fl}$) by flippase-based recombination of the *Adam19*^{Venus} knockin

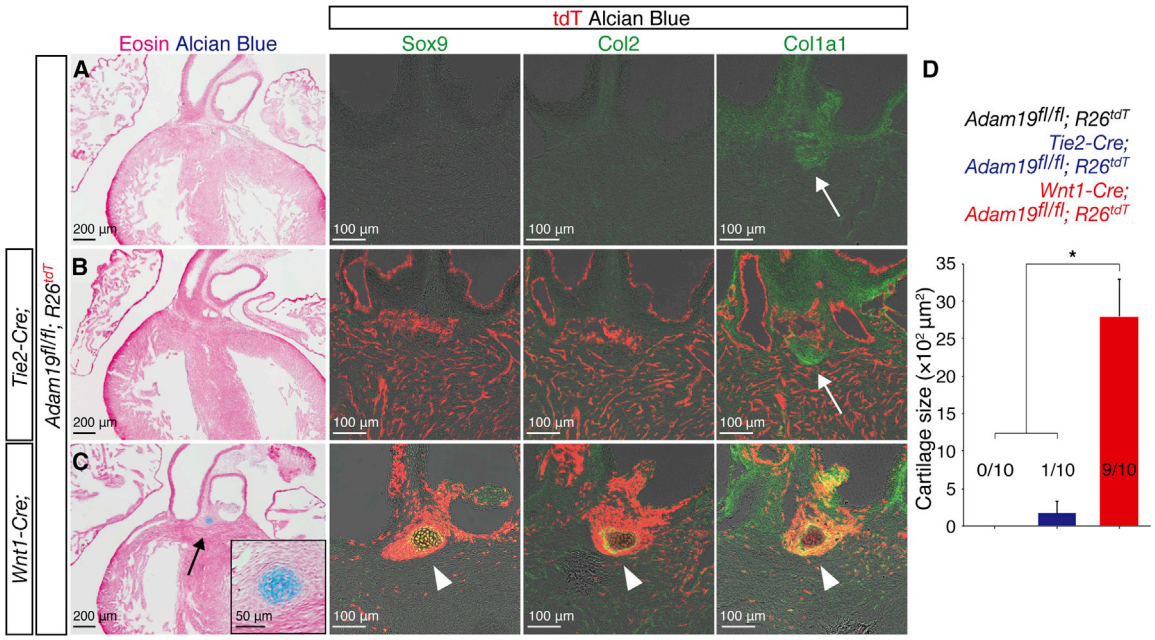

Figure 3. Adam19 Expression in CNCCs Is Required for Their Proper Cell Fate Decision

(A–C) Images of *Adam19*$^{fl/fl}$;*R26*^{tdT} (A), *Tie2-Cre;Adam19*$^{fl/fl}$;*R26*^{tdT} (B), and *Wnt1-Cre;Adam19*$^{fl/fl}$;*R26*^{tdT} (C) hearts at E18.5. Eosin and Alcian blue staining (left panels); a black arrow indicates the ectopic cartilage. Alcian blue-stained sections immunostained for chondrocyte and tenocyte markers (right panels); white arrows indicate Col1a1^{+} tenocyte-like cells and arrowheads indicate ectopic cartilages.

(D) Quantification of cartilage sizes in *Adam19*$^{fl/fl}$;*R26*^{tdT}, *Tie2-Cre;Adam19*$^{fl/fl}$;*R26*^{tdT}, and *Wnt1-Cre;Adam19*$^{fl/fl}$;*R26*^{tdT} hearts at E18.5. The numbers of hearts with ectopic cartilage per that of analyzed hearts (n = 10 per genotype) are shown. The data are presented as means ± SEMs; *p < 0.05.

See also Figure S3.

allele (Figures S1A and S1C). Adam19 was expressed both in endothelial cells and CNCCs during heart development (Figures 1A and S2A); therefore, we bred *Tie2-Cre* or *Wnt1-Cre* mice with *Adam19*$^{fl/fl}$ and *R26*^{tdT} reporter mice (*Adam19*$^{fl/fl}$;*R26*^{tdT}). None of the *Adam19*$^{fl/fl}$;*R26*^{tdT} embryos (0/10) and only one of the *Tie2-Cre;Adam19*$^{fl/fl}$;*R26*^{tdT} embryos (1/10) showed Alcian blue-stained nodules, and their cells in the AP septum were positive for the tenocyte marker Col1a1 at E18.5 (Figures 3A and 3B, arrows). In contrast, the majority of *Wnt1-Cre;Adam19*$^{fl/fl}$;*R26*^{tdT} mice (9/10) developed ectopic cardiac cartilages, which also were significantly larger than those of the other genotypes (Figures 3C and 3D). Immunostaining of *Wnt1-Cre;Adam19*$^{fl/fl}$;*R26*^{tdT} hearts revealed NCC-derived cartilages, which were surrounded by Col1a1^{+} tenocyte-like cells, indicating that these mice recapitulated the cartilage phenotype of *Adam19*-constitutive knockout mice (Figures 2 and 3C). These results suggest that Adam19 expression in CNCCs is required for the inhibition of the chondrogenic program in a cell-autonomous manner.

Defects in NCC patterning led to the homeotic transformation of original skeletal parts (Minoux and Rijli, 2010). However, *Adam19*$^{-/-}$ embryos had no gross abnormality in skeletal patterning at E18.5 (Figures S3A–S3C), and there was no significant difference in the distribution of *Adam19*$^{+/+}$ and *Adam19*$^{-/-}$ CNCCs (Figures S3D–S3F), indicating that Adam19 is involved in the local cell fate specification of CNCCs rather than in NCC patterning or migration.

Adam19-Deficient CNCCs Exhibit Sox9 Upregulation Before Abnormal Cartilage Formation

To elucidate the molecular mechanisms underlying the cartilage phenotype of *Adam19*$^{-/-}$ mice, we performed gene expression profiling of CNCCs. Given that *Adam19* was strongly expressed in the hearts of WT mice at E13.5 (Figures 1A and 1C) and that cardiac cartilage appeared in *Adam19*$^{-/-}$ mice at E15.5 (Figure S2C), we analyzed gene expression in CNCCs from *Adam19*$^{+/+}$;*Wnt1-Cre;R26*^{tdT} and *Adam19*$^{-/-}$;*Wnt1-Cre;R26*^{tdT} hearts at E14.5. Although transcriptional profiles were, overall, similar between the two genotypes, *Adam19*$^{-/-}$ CNCCs exhibited notable upregulation of *Sox9* transcripts compared with *Adam19*$^{+/+}$ CNCCs by the weighted average difference (WAD) method (Kadota et al., 2008; Figure 4A; Table S1), suggesting that Adam19 negatively regulates Sox9 expression in CNCCs.

Sox9 and Scx are key transcription factors that regulate chondrocyte and tenocyte differentiation, respectively (Akiyama et al., 2002; Mori-Akiyama et al., 2003; Murchison et al., 2007). Common precursor cells are both Sox9^{+} and Scx^{+} and form the junction between cartilage and a tendon/ligament (Sugimoto et al., 2013b). Immunohistochemical analysis showed that at E14.5, most *Adam19*$^{+/+}$ and *Adam19*$^{-/-}$ CNCCs in the AP septum expressed both Scx and Sox9 (Figure 4B), indicating that these CNCCs included Scx^{+}Sox9^{+} progenitors with both tenogenic and chondrogenic features. However, Sox9 protein expression was slightly higher in *Adam19*$^{-/-}$ than in *Adam19*$^{+/+}$ CNCCs, which was consistent with the microarray data (Figures 4A and

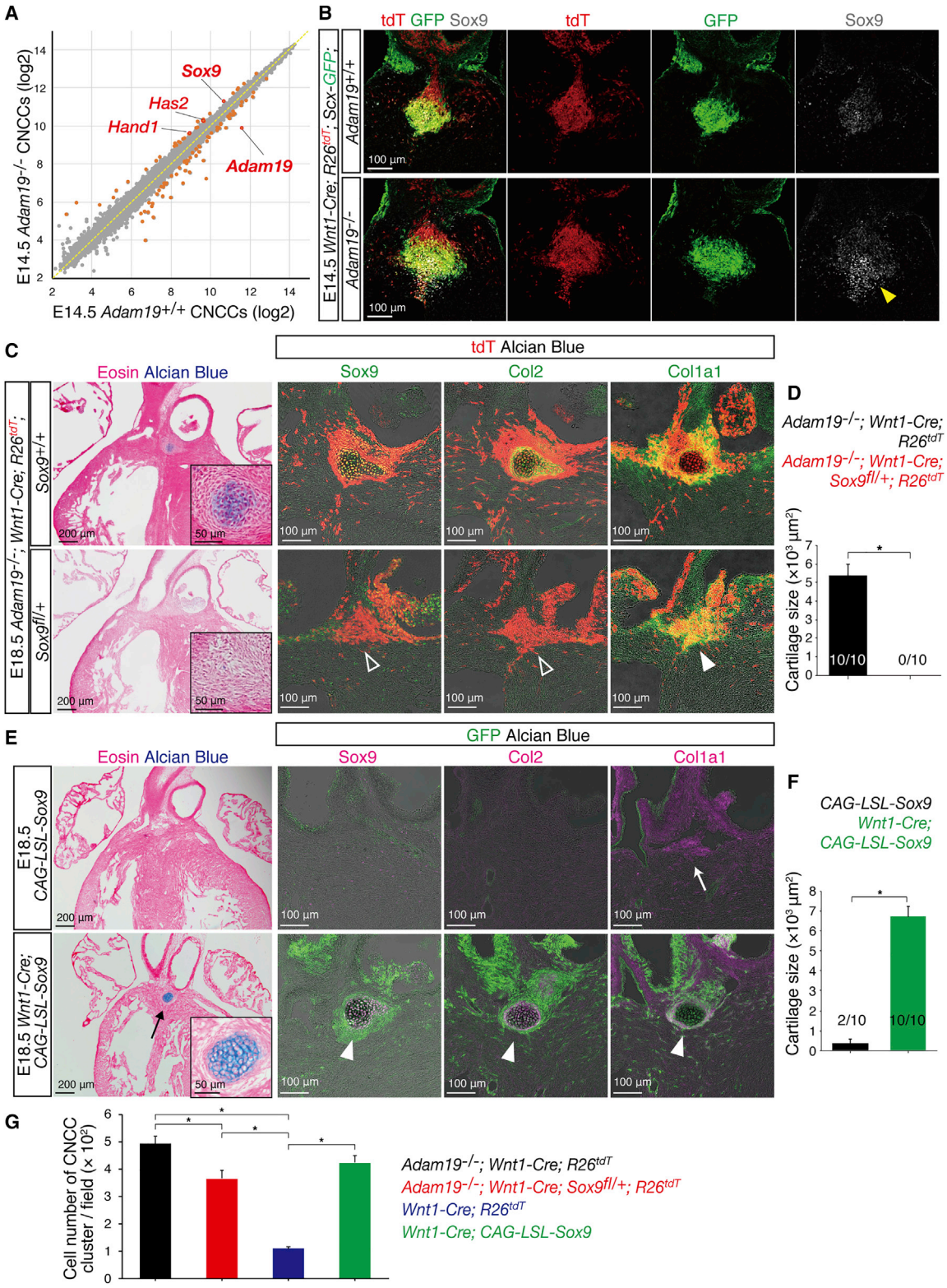

Figure 4. Sox9 Upregulation in *Adam19*-Deficient CNCCs Is Crucial for Abnormal Cardiac Cartilage Formation

(A) Scatterplot of microarray data for *Adam19*$^{+/+}$ and *Adam19*$^{-/-}$ CNCCs at E14.5; 100 most differentially expressed genes (orange dots) were identified by the WAD method. See also Table S1.

(legend continued on next page)

4B, arrowhead). In control *Adam19*$^{+/+}$ mice, the number of Sox9^{+} CNCCs gradually decreased at E16.5–E18.5, whereas in *Adam19*$^{-/-}$ mice, their number increased and remained high at the center of the CNCC cluster, where cartilage formation was observed (Figure S4).

Sox9 is the earliest marker for chondrogenic progenitor cells also expressed at the prechondrogenic condensation stage, a pivotal step in chondrogenesis (Hall and Miyake, 2000). To investigate whether the appearance of cartilaginous nodules in *Adam19*$^{-/-}$ hearts was related to abnormal prechondrogenic condensation, we examined the condensation of WT and *Adam19*$^{-/-}$ CNCCs. Staining with peanut agglutinin (PNA), a marker for mesenchymal cell aggregation, revealed that both WT and *Adam19*$^{-/-}$ CNCC clusters exhibited cell condensation at E14.5 (Figures S5A and S5B), suggesting that Adam19 deficiency does not affect CNCC condensation.

To further dissect the role of Adam19 in CNCCs, we assessed cell proliferation and apoptosis by Ki67 and TUNEL staining, respectively. The results revealed that *Adam19*$^{-/-}$ CNCCs exhibited enhanced local proliferation and no significant changes in apoptosis in the AP septum at E16.5 (Figures S5C–S5E), indicating that the failure to suppress *Sox9* expression in *Adam19*$^{-/-}$ mice could be related to abnormal differentiation and proliferation of NCC-derived Scx^{+}Sox9^{+} progenitors.

Sox9 Expression Levels Are Crucial for Cardiac Cartilage Formation

To test the hypothesis that ectopic cardiac cartilage production in *Adam19*$^{-/-}$ CNCCs was due to Sox9 upregulation, we investigated whether the reduction of *Sox9* gene dosage in CNCCs could rescue the cardiac cartilage phenotype in *Adam19*$^{-/-}$ mice by introducing a conditional floxed *Sox9* allele (*Sox9*$^{fl/+}$) (Kist et al., 2002). Although CNCCs of *Adam19*$^{-/-}$*;Wnt1-Cre;Sox9*$^{fl/+}$*;R26*^{tdT} mice migrated into the heart and formed CNCC clusters at the AP septum similar to those of *Adam19*$^{-/-}$*;Wnt1-Cre;R26*^{tdT} mice, abnormal cartilage formation and chondrogenic features such as Col2 expression were completely abolished in *Adam19*$^{-/-}$ CNCCs with reduced *Sox9* expression (Figures 4C and 4D), and their differentiation into Col1a1-expressing tenocyte-like cells in the AP septum was recovered (Figure 4C). The rescue of the ectopic cartilage phenotype in *Adam19*$^{-/-}$ hearts by *Sox9* downregulation in CNCCs indicates that the abnormal Col2 expression and chondrogenic differentiation in *Adam19*$^{-/-}$ CNCCs were induced by high Sox9 expression levels.

Conversely, we also investigated whether *Sox9* overexpression in CNCCs could induce ectopic cardiac cartilage formation using transgenic *CAG-LoxP-Stop-LoxP-Sox9-IRES-EGFP* (*CAG-LSL-Sox9*) mice overexpressing *Sox9* in a Cre-dependent manner (Kim et al., 2011). *Wnt1-Cre;CAG-LSL-Sox9* mice exhibited the CNCC-derived cardiac cartilage with elevated expression of chondrogenic markers Sox9 and Col2 at the same locations as in *Adam19*$^{-/-}$ mice (Figures 4E and 4F), but had no gross abnormality in original skeletal elements at E18.5 (Figure S6), indicating that Sox9 overexpression recapitulated the cardiac cartilage phenotype of *Adam19*$^{-/-}$ mice. Thus, high Sox9 expression in CNCCs is necessary and sufficient for ectopic Col2 expression and abnormal cartilage formation in the developing heart, suggesting that Adam19 inhibits cardiac chondrogenesis via suppressing *Sox9* expression.

To further investigate whether cell proliferation in *Adam19*$^{-/-}$ CNCCs (Figures S5E) was influenced by Sox9 expression levels, we counted the cell numbers in CNCC clusters of relevant mutants. Reduced Sox9 expression levels in *Adam19*$^{-/-}$ CNCCs caused a significant decrease in the number of cells present in the CNCC cluster, whereas Sox9 overexpression in NCC-lineage cells significantly increased the cell number (Figure 4G), indicating that the increased cell numbers in *Adam19*$^{-/-}$ CNCC clusters are at least partially due to Sox9 upregulation.

Alk2 Is a Candidate Substrate of Adam19 in Developing CNCCs

BMP signaling is one of the major pathways regulating chondrogenesis through Sox9 expression (Zeng et al., 2002), and our microarray analysis showed that *Adam19*$^{-/-}$ CNCCs exhibited increased transcription of BMP-regulated genes such as *Hand1* (Bonilla-Claudio et al., 2012; Vincentz et al., 2016) and *Has2* (Ma et al., 2005; Figure 4A; Table S1). Therefore, we next examined the activation of BMP signaling in CNCCs. BMP ligand-receptor interaction increases the kinase activity of type I receptors, leading to the phosphorylation of Smad1, Smad5, and Smad9 and downstream transcriptional changes (Wang et al., 2014), and we observed an increase in phospho-Smad^{+} cells among *Adam19*$^{-/-}$ CNCCs at E14.5 (Figure 5A), indicating enhanced BMP signaling.

Proteases of the ADAM family have been reported to participate in ectodomain shedding of transforming growth factor β (TGF-β)/BMP receptors and inhibit their signaling cascades (Hurst et al., 2017; Liu et al., 2009). These findings, together with our results on the requirement of Adam19 in CNCCs

(B) Heart sections were immunostained for GFP and Sox9. An arrowhead indicates Sox9^{+} CNCCs in the *Adam19*$^{-/-}$ heart. See also Figures S4 and S5.
(C) Absence of ectopic cartilage formation in *Adam19*$^{-/-}$*;Wnt1-Cre;Sox9*$^{fl/+}$*;R26*^{tdT} hearts was detected by eosin and Alcian blue staining and immunostaining for chondrocyte markers Sox9 and Col2 and tenocyte markers Col1a1 ($n \geq 3$ embryos per panel). Insets show higher-magnification views of CNCC cluster regions. *Adam19*$^{-/-}$ CNCCs with downregulated Sox9 expression lost chondrogenic features (open arrowheads) and recovered the original tenogenic feature (closed arrowhead).
(D) Quantification of maximum cartilage sizes at E18.5. The numbers of embryos with abnormal cartilages per that of analyzed embryos ($n = 10$) are shown.
(E) Ectopic cartilage formation in *Wnt1-Cre;CAG-LSL-Sox9* hearts was assessed by eosin and Alcian blue staining and immunostaining for Sox9, Col2, and Col1a1 ($n \geq 3$ embryos per panel). A black arrow indicates the ectopic cartilage; a magnified view is shown in the inset. A white arrow indicates Col1a1^{+} tenocyte-like cells and arrowheads indicate ectopic cartilage.
(F) Quantification of maximum cartilage sizes at E18.5. The numbers of embryos with abnormal cartilages per those of analyzed embryos ($n = 10$) are shown.
(G) Quantification of the cell numbers in CNCC clusters per section at E18.5 ($n = 8$ embryos per genotype).
The data are presented as means ± SEMs; *$p < 0.05$.
See also Figure S6.

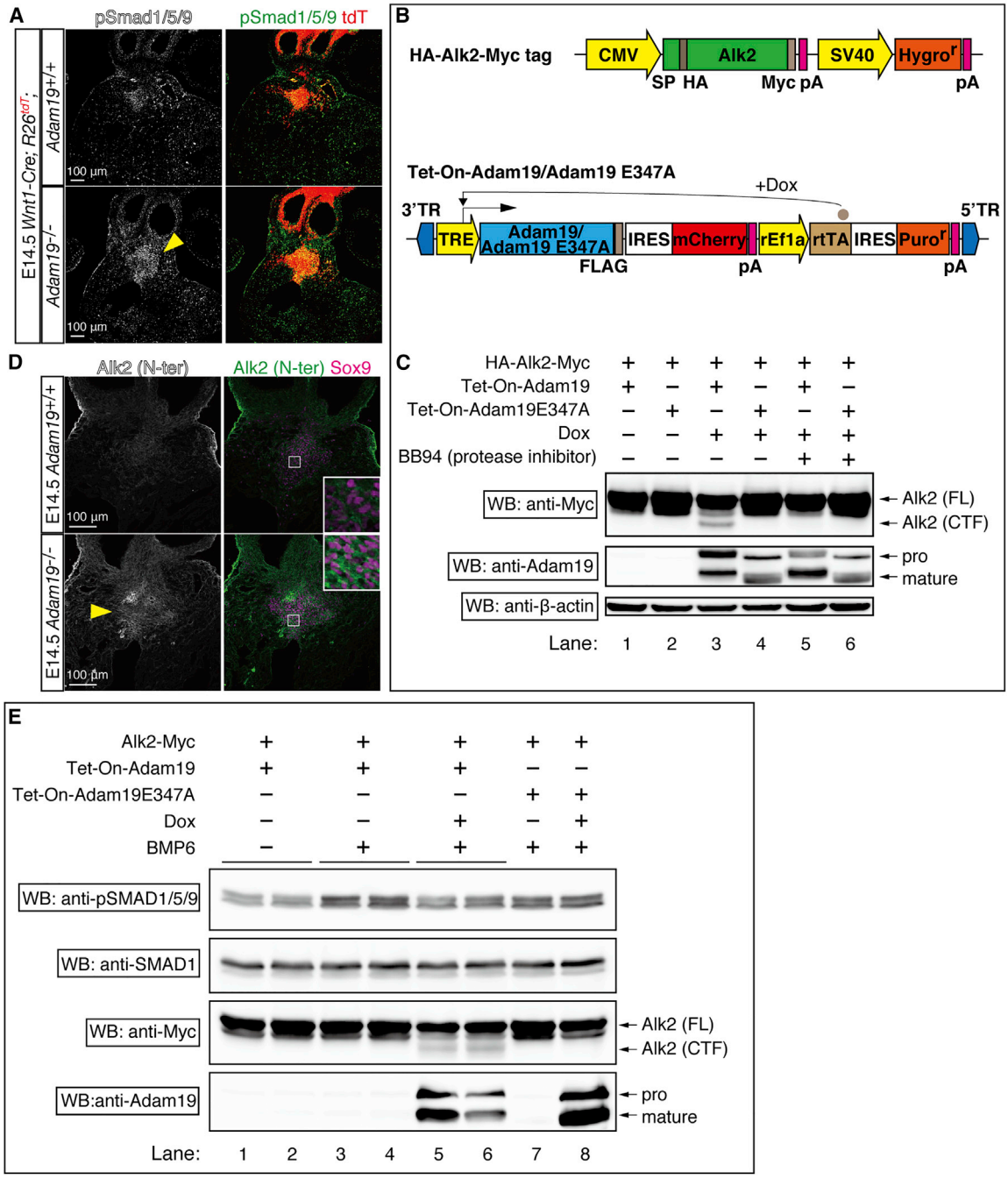

Figure 5. Alk2 Is a Candidate Substrate of Adam19 in Developing CNCCs

(A) Heart sections were immunostained for phospho-Smad1/5/9 (n = 3 embryos per genotype). An arrowhead indicates increased Smad1/5/9 phosphorylation in *Adam19*$^{-/-}$ CNCCs.

(B) Schematic representation of the expression vectors. SP, signal peptide; 3′/5′ TR, *piggyBac* terminal repeats.

(C) HEK293T cells co-expressing HA-Alk2-Myc with Tet-on-Adam19 or Tet-on-Adam19 E347A were incubated or not with doxycycline (Dox) and protease inhibitor BB94 and analyzed by western blotting with the indicated antibodies.

(D) Heart sections were immunostained for Alk2 (N-terminal region) and Sox9 (n = 3 embryos per genotype). Boxed areas are enlarged in the insets.

(E) HEK293T cells co-expressing Alk2-Myc with Tet-on-Adam19 or Tet-on-Adam19 E347A were incubated with or without Dox and BMP6 and analyzed by western blotting with the indicated antibodies. Alk2 protein was abundant in *Adam19*$^{-/-}$ CNCCs (arrowhead). CTF, C-terminal fragment; FL, full length; pro and mature, proenzyme and mature forms of Adam19, respectively.

See also Figure S7.

(Figures 3C and 3D) and the enhanced BMP signaling in *Adam19*$^{-/-}$ CNCCs (Figures 4A and 5A), suggest that Adam19 may act through the cleavage of BMP receptors, thus inhibiting BMP signaling in CNCCs. To test this hypothesis, we co-expressed Adam19 with the C-terminally Myc-tagged BMP receptors (Bmpr1a, Bmpr1b, Bmpr2, and Alk2) in HEK293T cells (Figure S7A, top panel). The short fragment indicative of receptor cleavage was detected only in cells co-expressing Adam19 with Alk2 but not with other BMP receptors (Figure S7A, red arrowhead); however, Alk2 was not cleaved in cells expressing protease-inactive Adam19 E347A (Figure S7A, lane 8). These observations were further confirmed using the Tet-on system, which enabled the induction of Adam19 expression by doxycycline (Dox) (Kim et al., 2016; Figure 5B). The short Alk2 fragment was not detected in Dox^{-} control cells (Figure 5C, lanes 1 and 2) or cells expressing Adam19 E347A (Figure 5C, lane 4) and appeared only in those expressing Adam19 WT (Figure 5C, lane 3), but disappeared after treatment with metalloprotease inhibitor BB94 (Figure 5C, lane 5). These findings indicated that Adam19 selectively induced Alk2 ectodomain shedding in HEK293T cells.

We next asked whether human (h)ADAM19 also has a function to mediate the ectodomain shedding of hALK2. HEK293T cells co-expressing hALK2 and hADAM19 but not the hADAM19 E346A mutant demonstrated the cleavage of hALK2, which was inhibited by BB94 (Figure S7B), indicating that Adam19-mediated Alk2 processing is conserved from mice to humans.

Alk2 expression is required for CNCC migration to the cardiac outflow tract, where it is detected at E11.5 (Kaartinen et al., 2004), suggesting the presence of Alk2 in postmigratory CNCCs. Immunohistochemistry analysis using an antibody against the Alk2 N terminus revealed that Alk2 protein was abundantly present at the Sox9^{+} region of the AP septum in the *Adam19*$^{-/-}$ hearts, but not in WT hearts at E14.5 (Figure 5D), indicating the accumulation of uncleaved Alk2 protein in *Adam19*$^{-/-}$ hearts.

Adam19 Reduces the Responsiveness to BMP6 in Alk2-Expressing Cells

We next examined the response to a BMP ligand in Alk2-expressing HEK293T cells with and without Adam19. Given that Alk2 binds BMP6 and BMP7 (Lavery et al., 2008; Macías-Silva et al., 1998; Saremba et al., 2008) and that *Bmp6;Bmp7* double-knockout mice have defects in outflow tract formation, valve morphogenesis, and ventricular septum (Kim et al., 2001), similar to those in *Adam19* or *Alk2* mutants (Kaartinen et al., 2004; Kurohara et al., 2004; Thomas et al., 2012; Zhou et al., 2004), we used BMP6 as an Alk2 ligand in heart development. BMP6 administration increased the level of phospho-Smad1/5/9 in Alk2-Myc-expressing HEK293T cells (Figure 5E, lanes 3 and 4) compared to untreated cells (Figure 5E, lanes 1 and 2), which was attenuated by Adam19 induction, followed by Alk2 processing (Figure 5E, lanes 5 and 6). However, Smad1/5/9 phosphorylation was not influenced by Adam19 E347A expression (Figure 5E, lanes 7 and 8). These data indicate that Adam19-mediated Alk2 ectodomain shedding reduces cellular responsiveness to the BMP ligand *in vitro*.

BMP Type I Receptor Inhibition Abolishes the Ectopic Cartilage Phenotype in *Adam19*$^{-/-}$ Hearts

A constitutively activating mutation in *ALK2* causes fibrodysplasia ossificans progressiva (FOP) in humans, which manifests by ectopic endochondral bone formation with increased phosphorylation of Smad1/5/9 (Kaplan et al., 2012; Yu et al., 2008), similar to the phenotype of *Adam19*$^{-/-}$ hearts. As CNCC migration to the outflow tract is disrupted in Alk2 knockout or conditional knockout mice (Kaartinen et al., 2004), these models could not be applied to study CNCCs in the AP septum. We, therefore, used LDN-193189, a selective inhibitor of BMP type I receptor, which can reduce heterotopic ossification in the FOP mouse model with constitutively active Alk2 (Cuny et al., 2008; Yu et al., 2008). To investigate whether aberrant Bmp-Alk2 signaling was a cause of the ectopic cartilage formation in *Adam19*$^{-/-}$ mice, we treated mutant mice with LDN-193189 at E14.25–E16.25—in other words, from the end of CNCC migration until the decrease of Adam19 expression in the AP septum (Figures 6A and S2A). Inhibition of BMP type I receptor in *Adam19*$^{-/-}$*;Wnt1-Cre;R26*^{tdT} embryos rescued the ectopic cartilage phenotype accompanying marked reductions in Sox9 and Col2 expression while recovering Col1a1 expression (Figures 6B and 6C), suggesting that aberrant Sox9 expression and cardiac cartilage formation in *Adam19*$^{-/-}$ CNCCs depended on BMP signaling.

To confirm that the reduction of Sox9 levels by the BMP inhibitor was essential for eliminating the cardiac cartilage phenotype, we also administered LDN-193189 to *Sox9*-overexpressing (*Wnt1-CreCAG-LSL-Sox9*) mice. Because NCCs of *Wnt1-CreCAG-LSL-Sox9* mice expressed exogenous Sox9 before the start of LDN-193189 administration, we confirmed that these mice had no ectopic cartilage nodules in the hearts before treatment (Figure 6D). In contrast to *Adam19*$^{-/-}$ mice, all of the *Sox9*-overexpressing mice displayed cartilaginous nodules in the heart after LDN-193189 treatment (Figures 6C and 6E), indicating that aberrant BMP signaling induced cardiac cartilage formation in Adam19-deficient CNCCs by upregulating Sox9 expression.

DISCUSSION

This study reveals a mechanism suppressing the chondrogenic fates of NCCs; a transmembrane metalloprotease Adam19 mediates the ectodomain shedding of BMP type I receptor Alk2 and negatively regulates BMP signaling in CNCCs in a cell-autonomous manner, thereby preventing aberrant Sox9 expression and subsequent ectopic cartilage formation in the developing heart (Figure 7).

BMP signaling through Alk2 is required for CNCC migration and outflow tract formation during heart development (Kaartinen et al., 2004). Our data suggest that Adam19 attenuates the response of CNCCs to BMP ligands (Figure 5), which is critical for local specification of their fate after migration to the AP septum of the heart (Figure 6). In our model (Figure 7), CNCC fate is determined by the balance between BMP-Alk2 signaling and Adam19-mediated proteolytic regulation in a spatiotemporally specific manner. The formation of

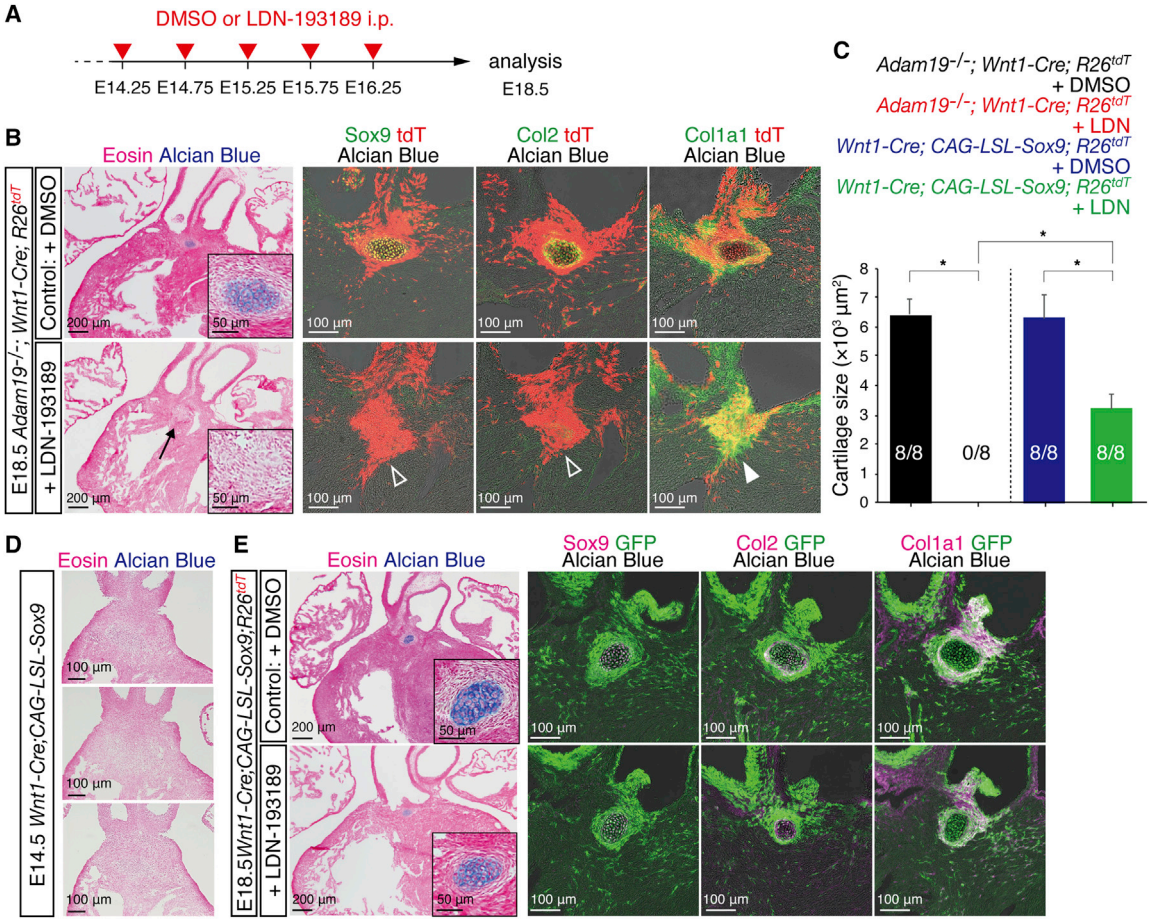

Figure 6. BMP Type I Receptor Inhibition Abolishes the Ectopic Cartilage Phenotype in *Adam19*$^{-/-}$ Hearts

(A) Schedule of LDN-193189 administration.

(B) Eosin and Alcian blue staining; insets show high-magnification views of CNCC clusters; a black arrow indicates the target area without cartilage (left panels). Alcian blue-stained heart sections were immunostained for chondrocyte and tenocyte markers ($n \geq 3$ embryos per panel); open arrowheads indicate cartilage markers and a closed arrowhead indicates the tendinous CNCC cluster (right panels).

(C) Quantification of the maximum cartilage sizes in the hearts of DMSO- or LDN-193189-treated *Adam19*$^{-/-}$;*Wnt1-Cre;R26*^{tdT} and *Wnt1-Cre;CAG-LSL-Sox9;R26*^{tdT} mice at E18.5. The numbers of embryos with abnormal cartilages per the total number of analyzed embryos (n = 8) are shown. The data are presented as means ± SEMs; *$p < 0.05$.

(D) Eosin/Alcian blue staining of E14.5 *Wnt1-Cre;CAG-LSL-Sox9* heart sections did not reveal any Alcian blue^{+} nodules before LDN-193189 administration (n = 3 embryos).

(E) Eosin- and Alcian blue-stained heart sections of DMSO- or LDN-193189-treated *Wnt1-Cre;CAG-LSL-Sox9;R26*^{tdT} mice at E18.5; insets show high-magnification views of CNCC clusters (left panels). Alcian blue-stained heart sections were immunostained for chondrocyte and tenocyte markers (right panels; $n \geq 3$ embryos per panel).

rudimentary cartilaginous nodules in control WT, *Adam19*$^{+/-}$, and *CAG-LSL-Sox9* hearts does not contradict this model and implies that the role of Adam19-dependent regulation is basically to minimize chondrogenic differentiation in CNCCs, which was abrogated in most cases as a consequence of Adam19-mediated proteolysis (Figures 1E, 4F, and 7).

Several proteins were shown to inhibit the skeletogenic differentiation of NCCs in mice. Neural crest stem cell transcription factor Sox10 negatively affected the mesenchymal fate decision of NCCs (John et al., 2011), whereas the deficiency of lysine *N*-methyltransferase Ezh2 provoked the massive derepression of *Hox* genes and downregulated the skeletogenic genes *Col2*, *Runx2*, *Osterix*, and *ALP*, but not *Sox9* in the first branchial arch containing skeletogenic NCCs (Schwarz et al., 2014). Unlike derepressed Hox proteins, Adam19 inhibits signaling along the BMP-Sox9 axis and reduces the expression of its downstream target gene *Col2* (Bell et al., 1997), thereby suppressing the chondrogenic potential of CNCCs (Figures 4, 5, and 6). At the same time, the ectopic cartilage was observed in mice with *Sox9*-overexpressing NCCs only in the heart but not in other tissues, at least during embryogenesis (Figures 4E, 4F, and S6), suggesting that fate restriction through Sox9 downregulation is a cardiac-specific mechanism; therefore, Adam19 is required in CNCCs and is involved in a mechanism that is distinct from that regulated by Hox proteins. Our data support the notion

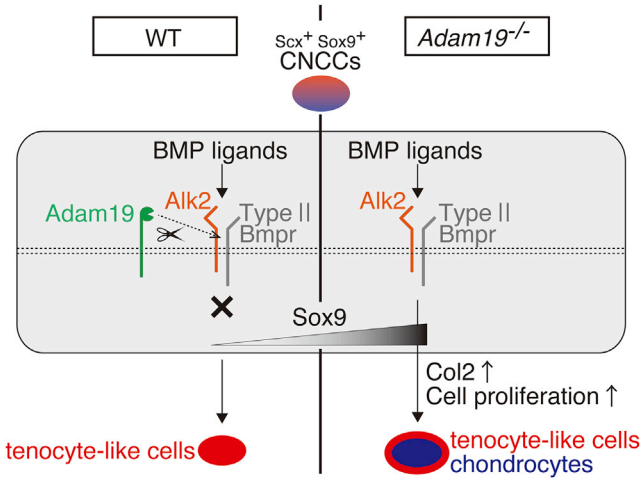

Figure 7. Schematic Representation of the Adam19-Dependent Fate Restriction Pathway in CNCCs

Postmigratory CNCCs clustering at the AP septum represent Scx^+Sox9^+ tenochondrogenic progenitors, in which Adam19 suppresses BMP signaling and expression of its target *Sox9* gene by proteolytic processing of BMP type I receptor Alk2; as a result, CNCCs differentiate into $Col1a1^+$ tenocyte-like cells. In the absence of Adam19, BMP signaling and Sox9 expression in CNCCs are not inhibited, resulting in CNCC differentiation into $Col2^+$ chondrocytes and ectopic cartilage formation in the heart.

that the limitation of the NCC skeletogenic potential is controlled by distinct molecular pathways that determine position-specific NCC fate during embryogenesis.

Several mechanisms can be conceived about the limited effects of *Wnt1-Cre;CAG-LSL-Sox9*. The first is that Sox9 protein levels are regulated by ubiquitin-proteasomal degradation (Akiyama et al., 2005; Hattori et al., 2013). Also, Sox9 can be stabilized by Snai2 (Luanpitpong et al., 2016). Therefore, excessive Sox9 proteins in NCCs may be degraded by the proteasome. The second is that in the posterior part of NCCs, we did not observe the cell condensation, which is a pivotal step in skeletal development (Hall and Miyake, 2000). Therefore, we could observe the ectopic cartilage formation only in the heart. Third, the promotor activity of *CAG-LSL-Sox9* is not very high. The levels of Sox9 mRNA in *Sox9-Cre;CAG-LSL-Sox9* is ~1.5 times higher than WT (Kim et al., 2011).

A recent study in chickens showed that a defined set of genes (*Sox8*, *Tfap2b*, and *Ets1*) encoding transcription factors that activate a cranial-specific *Sox10* enhancer could reprogram trunk NCCs to exhibit cranial neural crest identity with a chondrogenic potential (Simoes-Costa and Bronner, 2016). In mice, *Ets1* deficiency causes cardiac cartilage formation by NCCs similar to that in $Adam19^{-/-}$ mutants (Gao et al., 2010; Figure 2A). In our study, Adam19 knockout did not influence the expression of *Hox*, *Sox10*, *Sox8*, *Tfap2b*, *Ets1*, and *Fn1* in CNCCs at E14.5 (Figure 4A; Table S1); however, it is possible that Adam19 acts as a downstream effector of early NCC-specific genes, such as *Ets1*. Since Sox4 and Sox11 are required for the formation of the outflow tract and they can regulate Adam19 expression *in vitro* and *in vivo* (Paul et al., 2014), Adam19 gene expression is considered to be directly controlled by both Sox4 and Sox11 in the AP septum region.

Our CNCC microarray analysis did not reveal any downregulations of early NCC marker genes expressions (Figure 4A; Table S1), and NCC distribution was not impaired in Adam19-deficient mice (Figures S3D and S3E). It is possible that Adam10 mainly cleaves Cad6, and the Adam19 function is dispensable in premigratory NCCs in mice.

Our data showed that WT CNCCs in the AP septum display characteristics of tenocyte-like cells expressing Scx and Col1a1 (Figures 2C and 2D; Video S2), which raises an intriguing question of whether these tenogenic cells are also produced by other NCCs in different body parts. Further studies are required to address this issue. Although the roles of particular transcription factors, secreted signaling molecules, and epigenetic modifications in controlling NCC fate have been investigated (Simões-Costa and Bronner, 2015; Hu et al., 2014), our study suggests that the metalloprotease-mediated proteolytic control also participates in the regulatory mechanisms of NCC fate choice.

Defects in CNCCs lead to congenital heart abnormalities, including ventricular septal defects and abnormal valvulogenesis (Hutson and Kirby, 2007; Keyte and Hutson, 2012), which are commonly caused by the deficiency of *BMP6*/*BMP7*, *Alk2*, *Adam19*, and *Sox9* (Kaartinen et al., 2004; Kim et al., 2001; Kurohara et al., 2004; Thomas et al., 2012; Zhou et al., 2004; Akiyama et al., 2004). The hearts of $Adam19^{-/-}$ mice displayed hyperplastic valves and exhibited Sox9 upregulation (Figure 1D, asterisks), whereas *Alk2* deletion in the cushion mesenchyme resulted in bicuspid aortic valve formation and the downregulation of *Sox9* expression in aortic valves (Thomas et al., 2012; Wang et al., 2005). These pathological conditions could be explained by the disruption of regulated Sox9 expression and cell proliferation. Because Adam19 is also expressed by non-neural crest-derived cells in the heart (Figures 1A, S2A, and S2B) and ventricular septal defects were observed in only 3/10 hearts of NCC-specific Adam19 conditional knockout mice with mild hyperplastic valve phenotypes (data not shown), the Adam19-expressing non-neural crest-derived cells may also contribute to the formation of ventricular septa and valves during heart development.

In humans, cardiac cartilage formation is observed in heart diseases (Ferris and Aherne, 1971; McConnell, 1970), and hADAM19 is also expressed in the heart (Wei et al., 2001). Therefore, our hADAM19 data imply that human hearts possess ADAM19 function that prevents abnormal cardiac chondrogenesis (Figure S7B). Because Adam19 selectively mediates the processing of Alk2 and has inhibitory effects on BMP signaling cascades (Figures 5E and S7A), hADAM19-hALK2 results also raise the possibility that ADAM19 protein or ADAM19 activator administration can be a therapeutic strategy for human pediatric diseases associated with the constitutive activation of ALK2 (Figure S7B; Han et al., 2018). Thus, our findings yield insights into the mechanisms regulating NCC fate, as well as the etiologic and therapeutic implications of human diseases.

STAR★METHODS

Detailed methods are provided in the online version of this paper and include the following:

- KEY RESOURCES TABLE
- LEAD CONTACT AND MATERIALS AVAILABILITY
- EXPERIMENTAL MODEL AND SUBJECT DETAILS
  - Mice
  - Cells
- METHOD DETAILS
  - Cell Sorting
  - Quantitative PCR
  - Microarray Analysis
  - Histology and Immunostaining
  - Quantification of Cell Apoptosis and Proliferation
  - Cartilage Staining
  - Plasmids
  - Western Blotting Analysis
  - LDN-193189 Treatment
- QUANTIFICATION AND STATISTICAL ANALYSIS
- DATA AND CODE AVAILABILITY

SUPPLEMENTAL INFORMATION

Supplemental Information can be found online at https://doi.org/10.1016/j.celrep.2019.09.019.

ACKNOWLEDGMENTS

We are grateful to L. Sommer and S. Tajbakhsh for critical reading of the manuscript and to C.P. Blobel, A. Kakizuka, E. Mekada, R. Iwamoto, H. Kuroda, H. Watanabe, G. Kondoh, I. Onitsuka, Y. Uchida, and Y. Mukouyama for their valuable comments and support. We thank S. Iseki for the *Wnt1-Cre* mice, A. Miyawaki for the *Venus* gene, Howard Hughes Medical Institute (HHMI) investigator R. Tsien for *CAG-LSL-Sox9*, and X. Liu and all of the members of the Sehara-Fujisawa laboratory for helpful discussions. This work was supported by the Japan Society for the Promotion of Science KAKENHI grants (13J04661 and 15K21745, to H.N.A., and 16H04793, 15H05938, 15H05935, and 22122007, to A.S.-F.).

AUTHOR CONTRIBUTIONS

H.N.A. and A.S.-F. designed the experiments and wrote the manuscript. H.N.A. performed most of the experiments. H.N.A., F.S., and T.Y. conducted and analyzed the microarray experiments. H.N.A. and H.K. generated *Adam19*$^{Venus/+}$ and *Adam19*$^{fl/+}$ mice. K.W., Y.Y., C.S., H.A., and R.K. provided materials and tools. All of the authors discussed the results and have read the manuscript.

DECLARATION OF INTERESTS

The authors declare no competing interests.

Received: April 18, 2019
Revised: August 12, 2019
Accepted: September 5, 2019
Published: October 15, 2019

REFERENCES

Abzhanov, A., Tzahor, E., Lassar, A.B., and Tabin, C.J. (2003). Dissimilar regulation of cell differentiation in mesencephalic (cranial) and sacral (trunk) neural crest cells in vitro. Development *130*, 4567–4579.

Akiyama, H., Chaboissier, M.-C., Martin, J.F., Schedl, A., and de Crombrugghe, B. (2002). The transcription factor Sox9 has essential roles in successive steps of the chondrocyte differentiation pathway and is required for expression of Sox5 and Sox6. Genes Dev. *16*, 2813–2828.

Akiyama, H., Chaboissier, M., Behringer, R.R., Rowitch, D.H., Schedl, A., Epstein, J.A., and De Crombrugghe, B. (2004). Essential role of Sox9 in the pathway that controls formation of cardiac valves and septa. Proc. Natl. Acad. Sci. USA *101*, 6502–6507.

Akiyama, H., Kamitani, T., Yang, X., Kandyil, R., Bridgewater, L.C., Fellous, M., Mori-Akiyama, Y., and de Crombrugghe, B. (2005). The transcription factor Sox9 is degraded by the ubiquitin-proteasome system and stabilized by a mutation in a ubiquitin-target site. Matrix Biol. *23*, 499–505.

Bell, D.M., Leung, K.K., Wheatley, S.C., Ng, L.J., Zhou, S., Ling, K.W., Sham, M.H., Koopman, P., Tam, P.P., and Cheah, K.S. (1997). SOX9 directly regulates the type-II collagen gene. Nat. Genet. *16*, 174–178.

Bonilla-Claudio, M., Wang, J., Bai, Y., Klysik, E., Selever, J., and Martin, J.F. (2012). Bmp signaling regulates a dose-dependent transcriptional program to control facial skeletal development. Development *139*, 709–719.

Chen, D., Wang, X., Liang, D., Gordon, J., Mittal, A., Manley, N., Degenhardt, K., and Astrof, S. (2015). Fibronectin signals through integrin α5β1 to regulate cardiovascular development in a cell type-specific manner. Dev. Biol. *407*, 195–210.

Chesneau, V., Becherer, J.D., Zheng, Y., Erdjument-Bromage, H., Tempst, P., and Blobel, C.P. (2003). Catalytic properties of ADAM19. J. Biol. Chem. *278*, 22331–22340.

Creuzet, S., Couly, G., Vincent, C., and Le Douarin, N.M. (2002). Negative effect of Hox gene expression on the development of the neural crest-derived facial skeleton. Development *129*, 4301–4313.

Cuny, G.D., Yu, P.B., Laha, J.K., Xing, X., Liu, J.-F., Lai, C.S., Deng, D.Y., Sachidanandan, C., Bloch, K.D., and Peterson, R.T. (2008). Structure-activity relationship study of bone morphogenetic protein (BMP) signaling inhibitors. Bioorg. Med. Chem. Lett. *18*, 4388–4392.

Danielian, P.S., Muccino, D., Rowitch, D.H., Michael, S.K., and McMahon, A.P. (1998). Modification of gene activity in mouse embryos in utero by a tamoxifen-inducible form of Cre recombinase. Curr. Biol. *8*, 1323–1326.

Dupin, E., Calloni, G.W., Coelho-Aguiar, J.M., and Le Douarin, N.M. (2018). The issue of the multipotency of the neural crest cells. Dev. Biol. *444* (*Suppl 1*), S47–S59.

Etchevers, H.C., Vincent, C., Le Douarin, N.M., and Couly, G.F. (2001). The cephalic neural crest provides pericytes and smooth muscle cells to all blood vessels of the face and forebrain. Development *128*, 1059–1068.

Farley, F.W., Soriano, P., Steffen, L.S., and Dymecki, S.M. (2003). Widespread recombinase expression using FLPeR (flipper) mice. Genesis 2000 *28*, 106–110.

Ferris, J.A., and Aherne, W.A. (1971). Cartilage in relation to the conducting tissue of the heart in sudden death. Lancet *1*, 64–66.

Gao, Z., Kim, G.H., Mackinnon, A.C., Flagg, A.E., Bassett, B., Earley, J.U., and Svensson, E.C. (2010). Ets1 is required for proper migration and differentiation of the cardiac neural crest. Development *137*, 1543–1551.

Hall, B.K., and Miyake, T. (2000). All for one and one for all: condensations and the initiation of skeletal development. BioEssays *22*, 138–147.

Han, H.J., Jain, P., and Resnick, A.C. (2018). Shared ACVR1 mutations in FOP and DIPG: opportunities and challenges in extending biological and clinical implications across rare diseases. Bone *109*, 91–100.

Hattori, T., Kishino, T., Stephen, S., Eberspaecher, H., Maki, S., Takigawa, M., de Crombrugghe, B., and Yasuda, H. (2013). E6-AP/UBE3A protein acts as a ubiquitin ligase toward SOX9 protein. J. Biol. Chem. *288*, 35138–35148.

Hu, N., Strobl-Mazzulla, P.H., and Bronner, M.E. (2014). Epigenetic regulation in neural crest development. Dev. Biol. *396*, 159–168.

Hurst, L.A., Dunmore, B.J., Long, L., Crosby, A., Al-Lamki, R., Deighton, J., Southwood, M., Yang, X., Nikolic, M.Z., Herrera, B., et al. (2017). TNFα drives pulmonary arterial hypertension by suppressing the BMP type-II receptor and altering NOTCH signalling. Nat. Commun. *8*, 14079.

Hutson, M.R., and Kirby, M.L. (2007). Model systems for the study of heart development and disease. Cardiac neural crest and conotruncal malformations. Semin. Cell Dev. Biol. *18*, 101–110.

Jiang, X., Rowitch, D.H., Soriano, P., McMahon, A.P., and Sucov, H.M. (2000). Fate of the mammalian cardiac neural crest. Development *127*, 1607–1616.

John, N., Cinelli, P., Wegner, M., and Sommer, L. (2011). Transforming growth factor β-mediated Sox10 suppression controls mesenchymal progenitor generation in neural crest stem cells. Stem Cells *29*, 689–699.

Kaartinen, V., Dudas, M., Nagy, A., Sridurongrit, S., Lu, M.M., and Epstein, J.A. (2004). Cardiac outflow tract defects in mice lacking ALK2 in neural crest cells. Development *131*, 3481–3490.

Kadota, K., Nakai, Y., and Shimizu, K. (2008). A weighted average difference method for detecting differentially expressed genes from microarray data. Algorithms Mol. Biol. *3*, 8.

Kaplan, F.S., Chakkalakal, S.A., and Shore, E.M. (2012). Fibrodysplasia ossificans progressiva: mechanisms and models of skeletal metamorphosis. Dis. Model. Mech. *5*, 756–762.

Keyte, A., and Hutson, M.R. (2012). The neural crest in cardiac congenital anomalies. Differentiation *84*, 25–40.

Kim, R.Y., Robertson, E.J., and Solloway, M.J. (2001). Bmp6 and Bmp7 are required for cushion formation and septation in the developing mouse heart. Dev. Biol. *235*, 449–466.

Kim, Y., Murao, H., Yamamoto, K., Deng, J.M., Behringer, R.R., Nakamura, T., and Akiyama, H. (2011). Generation of transgenic mice for conditional overexpression of Sox9. J. Bone Miner. Metab. *29*, 123–129.

Kim, S.-I., Oceguera-Yanez, F., Sakurai, C., Nakagawa, M., Yamanaka, S., and Woltjen, K. (2016). Inducible Transgene Expression in Human iPS Cells Using Versatile All-in-One piggyBac Transposons. Methods Mol. Biol. *1357*, 111–131.

Kirby, M.L., Gale, T.F., and Stewart, D.E. (1983). Neural crest cells contribute to normal aorticopulmonary septation. Science *220*, 1059–1061.

Kisanuki, Y.Y., Hammer, R.E., Miyazaki, J., Williams, S.C., Richardson, J.A., and Yanagisawa, M. (2001). Tie2-Cre transgenic mice: a new model for endothelial cell-lineage analysis in vivo. Dev. Biol. *230*, 230–242.

Kist, R., Schrewe, H., Balling, R., and Scherer, G. (2002). Conditional inactivation of Sox9: a mouse model for campomelic dysplasia. Genesis 2000 *32*, 121–123.

Kiyonari, H., Kaneko, M., Abe, S., and Aizawa, S. (2010). Three inhibitors of FGF receptor, ERK, and GSK3 establishes germline-competent embryonic stem cells of C57BL/6N mouse strain with high efficiency and stability. Genesis *48*, 317–327.

Komatsu, K., Wakatsuki, S., Yamada, S., Yamamura, K., Miyazaki, J., and Sehara-Fujisawa, A. (2007). Meltrin beta expressed in cardiac neural crest cells is required for ventricular septum formation of the heart. Dev. Biol. *303*, 82–92.

Kovacic, J.C., Mercader, N., Torres, M., Boehm, M., and Fuster, V. (2012). Epithelial-to-mesenchymal and endothelial-to-mesenchymal transition: from cardiovascular development to disease. Circulation *125*, 1795–1808.

Kurohara, K., Komatsu, K., Kurisaki, T., Masuda, A., Irie, N., Asano, M., Sudo, K., Nabeshima, Y., Iwakura, Y., and Sehara-Fujisawa, A. (2004). Essential roles of Meltrin beta (ADAM19) in heart development. Dev. Biol. *267*, 14–28.

Lavery, K., Swain, P., Falb, D., and Alaoui-Ismaili, M.H. (2008). BMP-2/4 and BMP-6/7 differentially utilize cell surface receptors to induce osteoblastic differentiation of human bone marrow-derived mesenchymal stem cells. J. Biol. Chem. *283*, 20948–20958.

Le Douarin, N.M., and Kalcheim, C. (1999). The Neural Crest, Second Edition (Cambridge University Press).

Le Douarin, N.M., Creuzet, S., Couly, G., and Dupin, E. (2004). Neural crest cell plasticity and its limits. Development *131*, 4637–4650.

Levay, A.K., Peacock, J.D., Lu, Y., Koch, M., Hinton, R.B., Jr., Kadler, K.E., and Lincoln, J. (2008). Scleraxis is required for cell lineage differentiation and extracellular matrix remodeling during murine heart valve formation in vivo. Circ. Res. *103*, 948–956.

Li, J., Perfetto, M., Neuner, R., Bahudhanapati, H., Christian, L., Mathavan, K., Bridges, L.C., Alfandari, D., and Wei, S. (2018). *Xenopus* ADAM19 regulates Wnt signaling and neural crest specification by stabilizing ADAM13. Development *145*, dev158154.

Liu, C., Xu, P., Lamouille, S., Xu, J., and Derynck, R. (2009). TACE-mediated ectodomain shedding of the type I TGF-beta receptor downregulates TGF-beta signaling. Mol. Cell *35*, 26–36.

Luanpitpong, S., Li, J., Manke, A., Brundage, K., Ellis, E., McLaughlin, S.L., Angsutararux, P., Chanthra, N., Voronkova, M., Chen, Y.C., et al. (2016). SLUG is required for SOX9 stabilization and functions to promote cancer stem cells and metastasis in human lung carcinoma. Oncogene *35*, 2824–2833.

Ma, L., Lu, M.F., Schwartz, R.J., and Martin, J.F. (2005). Bmp2 is essential for cardiac cushion epithelial-mesenchymal transition and myocardial patterning. Development *132*, 5601–5611.

Macías-Silva, M., Hoodless, P.A., Tang, S.J., Buchwald, M., and Wrana, J.L. (1998). Specific activation of Smad1 signaling pathways by the BMP7 type I receptor, ALK2. J. Biol. Chem. *273*, 25628–25636.

Madisen, L., Zwingman, T.A., Sunkin, S.M., Oh, S.W., Zariwala, H.A., Gu, H., Ng, L.L., Palmiter, R.D., Hawrylycz, M.J., Jones, A.R., et al. (2010). A robust and high-throughput Cre reporting and characterization system for the whole mouse brain. Nat. Neurosci. *13*, 133–140.

McConnell, T.H. (1970). Bony and cartilaginous tumors of the heart and great vessels. Report of an osteosarcoma of the pulmonary artery. Cancer *25*, 611–617.

Minoux, M., and Rijli, F.M. (2010). Molecular mechanisms of cranial neural crest cell migration and patterning in craniofacial development. Development *137*, 2605–2621.

Minoux, M., Antonarakis, G.S., Kmita, M., Duboule, D., and Rijli, F.M. (2009). Rostral and caudal pharyngeal arches share a common neural crest ground pattern. Development *136*, 637–645.

Mori-Akiyama, Y., Akiyama, H., Rowitch, D.H., and de Crombrugghe, B. (2003). Sox9 is required for determination of the chondrogenic cell lineage in the cranial neural crest. Proc. Natl. Acad. Sci. USA *100*, 9360–9365.

Murchison, N.D., Price, B.A., Conner, D.A., Keene, D.R., Olson, E.N., Tabin, C.J., and Schweitzer, R. (2007). Regulation of tendon differentiation by scleraxis distinguishes force-transmitting tendons from muscle-anchoring tendons. Development *134*, 2697–2708.

Paul, M.H., Harvey, R.P., Wegner, M., and Sock, E. (2014). Cardiac outflow tract development relies on the complex function of Sox4 and Sox11 in multiple cell types. Cell. Mol. Life Sci. *71*, 2931–2945.

Renier, N., Wu, Z., Simon, D.J., Yang, J., Ariel, P., and Tessier-Lavigne, M. (2014). iDISCO: a simple, rapid method to immunolabel large tissue samples for volume imaging. Cell *159*, 896–910.

Saremba, S., Nickel, J., Seher, A., Kotzsch, A., Sebald, W., and Mueller, T.D. (2008). Type I receptor binding of bone morphogenetic protein 6 is dependent on N-glycosylation of the ligand. FEBS J. *275*, 172–183.

Schiffmacher, A.T., Padmanabhan, R., Jhingory, S., and Taneyhill, L.A. (2014). Cadherin-6B is proteolytically processed during epithelial-to-mesenchymal transitions of the cranial neural crest. Mol. Biol. Cell *25*, 41–54.

Schwarz, D., Varum, S., Zemke, M., Schöler, A., Baggiolini, A., Draganova, K., Koseki, H., Schübeler, D., and Sommer, L. (2014). Ezh2 is required for neural crest-derived cartilage and bone formation. Development *141*, 867–877.

Shirakabe, K., Wakatsuki, S., Kurisaki, T., and Fujisawa-Sehara, A. (2001). Roles of Meltrin beta/ADAM19 in the processing of neuregulin. J. Biol. Chem. *276*, 9352–9358.

Simões-Costa, M., and Bronner, M.E. (2015). Establishing neural crest identity: a gene regulatory recipe. Development *142*, 242–257.

Simoes-Costa, M., and Bronner, M.E. (2016). Reprogramming of avian neural crest axial identity and cell fate. Science *352*, 1570–1573.

Sugimoto, Y., Takimoto, A., Hiraki, Y., and Shukunami, C. (2013a). Generation and characterization of ScxCre transgenic mice. Genesis 2000 *51*, 275–283.

Sugimoto, Y., Takimoto, A., Akiyama, H., Kist, R., Scherer, G., Nakamura, T., Hiraki, Y., and Shukunami, C. (2013b). Scx+/Sox9+ progenitors contribute to the establishment of the junction between cartilage and tendon/ligament. Development *140*, 2280–2288.

Susaki, E.A., Tainaka, K., Perrin, D., Kishino, F., Tawara, T., Watanabe, T.M., Yokoyama, C., Onoe, H., Eguchi, M., Yamaguchi, S., et al. (2014). Whole-brain imaging with single-cell resolution using chemical cocktails and computational analysis. Cell *157*, 726–739.

Thomas, P.S., Sridurongrit, S., Ruiz-Lozano, P., and Kaartinen, V. (2012). Deficient signaling via Alk2 (Acvr1) leads to bicuspid aortic valve development. PLoS One *7*, e35539.

Vincentz, J.W., Casasnovas, J.J., Barnes, R.M., Que, J., Clouthier, D.E., Wang, J., and Firulli, A.B. (2016). Exclusion of Dlx5/6 expression from the distal-most mandibular arches enables BMP-mediated specification of the distal cap. Proc. Natl. Acad. Sci. USA *113*, 7563–7568.

Waldo, K., Miyagawa-Tomita, S., Kumiski, D., and Kirby, M.L. (1998). Cardiac neural crest cells provide new insight into septation of the cardiac outflow tract: aortic sac to ventricular septal closure. Dev. Biol. *196*, 129–144.

Wang, J., Sridurongrit, S., Dudas, M., Thomas, P., Nagy, A., Schneider, M.D., Epstein, J.A., and Kaartinen, V. (2005). Atrioventricular cushion transformation is mediated by ALK2 in the developing mouse heart. Dev. Biol. *286*, 299–310.

Wang, R.N., Green, J., Wang, Z., Deng, Y., Qiao, M., Peabody, M., Zhang, Q., Ye, J., Yan, Z., Denduluri, S., et al. (2014). Bone Morphogenetic Protein (BMP) signaling in development and human diseases. Genes Dis. *1*, 87–105.

Weber, S., and Saftig, P. (2012). Ectodomain shedding and ADAMs in development. Development *139*, 3693–3709.

Wei, P., Zhao, Y.G., Zhuang, L., Ruben, S., and Sang, Q.X. (2001). Expression and enzymatic activity of human disintegrin and metalloproteinase ADAM19/meltrin beta. Biochem. Biophys. Res. Commun. *280*, 744–755.

Yokozeki, T., Wakatsuki, S., Hatsuzawa, K., Black, R.A., Wada, I., and Sehara-Fujisawa, A. (2007). Meltrin beta (ADAM19) mediates ectodomain shedding of Neuregulin beta1 in the Golgi apparatus: fluorescence correlation spectroscopic observation of the dynamics of ectodomain shedding in living cells. Genes Cells *12*, 329–343.

Yu, P.B., Deng, D.Y., Lai, C.S., Hong, C.C., Cuny, G.D., Bouxsein, M.L., Hong, D.W., McManus, P.M., Katagiri, T., Sachidanandan, C., et al. (2008). BMP type I receptor inhibition reduces heterotopic [corrected] ossification. Nat. Med. *14*, 1363–1369.

Zeng, L., Kempf, H., Murtaugh, L.C., Sato, M.E., and Lassar, A.B. (2002). Shh establishes an Nkx3.2/Sox9 autoregulatory loop that is maintained by BMP signals to induce somitic chondrogenesis. Genes Dev. *16*, 1990–2005.

Zhou, H.M., Weskamp, G., Chesneau, V., Sahin, U., Vortkamp, A., Horiuchi, K., Chiusaroli, R., Hahn, R., Wilkes, D., Fisher, P., et al. (2004). Essential role for ADAM19 in cardiovascular morphogenesis. Mol. Cell. Biol. *24*, 96–104.

STAR★METHODS

KEY RESOURCES TABLE

REAGENT or RESOURCE	SOURCE	IDENTIFIER
Antibodies		
Rabbit polyclonal anti-Ki67	Abcam	Cat# ab15580; RRID:AB_443209
Goat polyclonal anti-GFP	Rockland	Cat# 600-101-215; RRID:AB_218182
Mouse monoclonal anti-Myh1 (MF20)	DSHB	AB_2147781; RRID:AB_2147781
Rat monoclonal anti-CD31	BD PharMingen	Cat# 550274; RRID:AB_393571
Rabbit polyclonal anti-Sox9	Millipore	Cat# AB5535; RRID:AB_2239761
Rabbit polyclonal anti-Aggrecan	Millipore	Cat# AB1031; RRID:AB_90460
Rabbit polyclonal anti-Col2	Abcam	Cat# ab34712; RRID:AB_731688
Rabbit polyclonal anti-SM22a (TAGLN)	Abcam	Cat# ab14106; RRID:AB_443021
Rabbit polyclonal anti-Col1a1	Bio-Rad	Cat# 2150-1410; RRID:AB_620433
Rabbit monoclonal anti-phospho-Smad1/5/9	Cell Signaling Technology	Cat# 13820; RRID:AB_2493181
Mouse monoclonal anti-Alk2	R&D Systems	Cat# MAB637; RRID:AB_2221997
Mouse monoclonal anti-Myc tag (9B11)	Cell Signaling Technology	Cat# 2276; RRID:AB_331783
Rabbit polyclonal anti-Adam19	(Shirakabe et al., 2001) Sehara lab	N/A
Mouse monoclonal anti-β-actin (AC-15)	Santa Cruz	Cat# sc-69879; RRID:AB_1119529
Mouse monoclonal anti-HA	Sigma-Aldrich	Cat# H3663; RRID:AB_262051
Rabbit monoclonal anti-Smad1 (D59D7)	Cell Signaling Technology	Cat# 6944; RRID:AB_10858882
Horse anti-mouse IgG, HRP-linked Antibody	Cell Signaling Technology	Cat#7076P2; RRID:AB_330924
Goat anti-rabbit IgG, HRP-linked Antibody	Cell Signaling Technology	Cat#7074P2; RRID:AB_2099233
Donkey anti-goat IgG (H+L) Cross-Adsorbed Secondary Antibody, Alexa Fluor 488	Thermo Fisher Scientific	Cat# A-11055; RRID:AB_142672
Donkey anti-mouse IgG (H+L) Highly Cross-Adsorbed Secondary Antibody, Alexa Fluor 594	Thermo Fisher Scientific	Cat# A-21203; RRID:AB_141633
Donkey polyclonal anti-mouse IgG (H+L) Highly Cross-Adsorbed Secondary Antibody, Alexa Fluor 647	Thermo Fisher Scientific	Cat# A-31571; RRID:AB_162542
Donkey anti-rabbit IgG (H+L) Highly Cross-Adsorbed Secondary Antibody, Alexa Fluor 488	Thermo Fisher Scientific	Cat# A-21206; RRID:AB_141708
Donkey anti-rabbit IgG (H+L) Highly Cross-Adsorbed Secondary Antibody, Alexa Fluor 594	Thermo Fisher Scientific	Cat# A-21207; RRID:AB_141637
Donkey anti-rabbit IgG (H+L) Highly Cross-Adsorbed Secondary Antibody, Alexa Fluor 647	Thermo Fisher Scientific	Cat# A-31573; RRID:AB_2536183
Donkey anti-rat IgG (H+L) Highly Cross-Adsorbed Secondary Antibody, Alexa Fluor 594	Thermo Fisher Scientific	Cat# A-21209; RRID:AB_2535795
Chemicals, Peptides, and Recombinant Proteins		
Alcian Blue 8GX	MP Biomedicals	Cat# 152624
Alizarin Red S	Wako	Cat# 011-01192
Fluorescein Labeled Peanut Agglutinin (PNA)	Vector Lab	Cat# FL-1071
Alexa Fluor 647 Phalloidin	Thermo Fisher Scientific	Cat# A22287
Benzyl Benzoate	Nacalai Tesque	Cat# 04601-65
Benzyl Alcohol	Nacalai Tesque	Cat# 045-21
Blocking One	Nacalai Tesque	Cat# 03953-95
Acetic Acid	Nacalai Tesque	Cat# 00212-85
Protease Inhibitor Cocktail	Nacalai Tesque	Cat# 25955-11
DAPI	Sigma-Aldrich	Cat# D9542-10MG

(*Continued on next page*)

Continued

REAGENT or RESOURCE	SOURCE	IDENTIFIER
LDN193189 Hydrochloride	Sigma-Aldrich	Cat# SML0559-25MG
FSC 22 Frozen Section Compound Clear	Leica	Cat# 3801480
TRIzol Reagent	Thermo Fisher Scientific	Cat# 15596026
Recombinant Human BMP-6 Protein	Peprotech	Cat# 120-06
Collagenase Type 2	Worthington	Cat# LS004176
Lipofectamine 2000 Transfection Reagent	Thermo Fisher Scientific	Cat# 11668019
Doxycycline Hyclate	LKT Labs	Cat# D5897
Bortezomib	LC laboratory	Cat# B-1408
Batimastat (BB94)	Med Chem express	Cat# HY-13564
Critical Commercial Assays		
Power SYBR Green PCR Master Mix	Thermo Fisher Scientific	Cat# 4368706
SuperScript VILO cDNA Synthesis Kit	Thermo Fisher Scientific	Cat# 11754050
RNeasy Plus Micro Kit	QIAGEN	Cat# 74034
ApopTag Plus *In Situ* Apoptosis Fluorescein Detection Kit	Millipore	Cat# S7111
Gateway BP Clonase II Enzyme mix	Thermo Fisher Scientific	Cat# 11789020
Gateway LR Clonase II Enzyme mix	Thermo Fisher Scientific	Cat# 11791020
ECL Prime Western Blotting Detection Reagent	GE Healthcare	Cat# RPN2232
Deposited Data		
Microarray in *Adam19*$^{+/+}$ and *Adam19*$^{-/-}$ CNCCs	This paper	GEO: GSE99551
Experimental Models: Cell Lines		
HEK293T	ATCC	Cat# CRL-11268
HK3i ES Cells	(Kiyonari et al., 2010)	N/A
Experimental Models: Organisms/Strains		
Mouse: *Adam19*$^{+/-}$	(Kurohara et al., 2004)	N/A
Mouse: *Wnt1-Cre*: *H2afv*$^{Tg(Wnt1\text{-}cre)11Rth}$	(Danielian et al., 1998)	MGI:2386570
Mouse: *Tie2-Cre*: *B6.Cg-Tg(Tek-cre)1Ywa*	RIKEN BRC (Kisanuki et al., 2001)	Cat # RBRC04495
Mouse: *R26*^{tdT}: *B6.Cg-Gt(ROSA)26Sor*$^{tm14(CAG\text{-}tdTomato)Hze}$*/J*	The Jackson Laboratory (Madisen et al., 2010)	Cat# 007914
Mouse: *Scx-GFP*	(Sugimoto et al., 2013a)	N/A
Mouse: *Sox9*$^{fl/fl}$	(Kist et al., 2002)	N/A
Mouse: *CAG-LSL-Sox9*: *B6.Cg-Tg(CAG-mRFP1,-SOX9,EGFP) 1Haak*	RIKEN BRC (Kim et al., 2011)	Cat # RBRC05654
Mouse: *Adam19*$^{Venus/+}$	This paper	N/A
Mouse: *Adam19*$^{fl/fl}$	This paper	N/A
Recombinant DNA		
pCMV3-C-Myc Negative Control Vector (C-terminal Myc-tagged)	Sino Biological Inc.	Cat# CV014
Mouse ALK-2/ACVR1 Gene ORF cDNA clone expression plasmid, C-Myc tag	Sino Biological Inc.	Cat# MG50297-CM
Mouse ALK-3 / BMPRIA ORF mammalian expression plasmid, C-Myc tag	Sino Biological Inc.	Cat# MG50078-CM
Mouse ALK-6 / BMPR1B Gene ORF cDNA clone expression plasmid, C-Myc tag	Sino Biological Inc.	Cat# MG50004-CM
Human ACVR1 cDNA ORF Clone C-Myc tag	Sino Biological Inc.	Cat# HG14875-CM
Human ADAM19 cDNA ORF Clone in Cloning Vector	Sino Biological Inc.	Cat# HG18760-U
pDONR221	Thermo Fisher Scientific	Cat# 12536017
PB-TAC-ERP2	(Kim et al., 2016)	Cat# 80478 (Addgene)/ Cat# RDB13246 (RIKEN BRC)
pCAG-PBase	(Kim et al., 2016)	Cat# RDB13241 (RIKEN BRC)

(*Continued on next page*)

Continued		
REAGENT or RESOURCE	SOURCE	IDENTIFIER
Software and Algorithms		
DP2-BSW software	Olympus	N/A
Volocity software	PerkinElmer	N/A
R statistical software (v3.1.2).	R Foundation for Statistical Computing	https://www.r-project.org/
LAS X software	Leica	N/A

LEAD CONTACT AND MATERIALS AVAILABILITY

Further information and requests for resources and reagents should be directed to and will be fulfilled by the Lead Contact, Atsuko Sehara-Fujisawa (sehara.atsuko.3m@kyoto-u.ac.jp). Mouse lines, plasmids, and other reagents generated in the study will be available upon request.

EXPERIMENTAL MODEL AND SUBJECT DETAILS

Mice

Generation of *Adam19*$^{-/-}$ (Kurohara et al., 2004), *Wnt1-Cre* (Danielian et al., 1998), *Tie2-Cre* (Kisanuki et al., 2001), *Rosa26*$^{CAG\text{-}LSL\text{-}tdTomato/+}$ (*R26*^{tdT}) (Madisen et al., 2010), *Scx-GFP* (Sugimoto et al., 2013a), *Sox9*$^{fl/fl}$ (Kist et al., 2002), and *CAG-LSL-Sox9-IRES-EGFP* (Kim et al., 2011) mice was previously described. *Adam19*$^{Venus/+}$ and *Adam19*$^{fl/+}$ mouse lines (Accession number CDB1228K: http://www2.clst.riken.jp/arg/mutant%20mice%20list.html) were established as follows. A bacterial artificial clone construct containing the mouse *Adam19* gene (ID: B6Ng01-116D03) was purchased from RIKEN BRC. The linearized targeting vector was transferred by electroporation into HK3i (C57BL/6 strain) embryonic stem cells (Kiyonari et al., 2010), and correctly targeted cell clones were identified by PCR and Southern blotting as described (http://www2.clst.riken.jp/arg/methods.html). Germline transmission was confirmed by PCR. *Adam19*$^{Venus/+}$ mice were bred with FLPeR mice (*R26*^{fki}) (Farley et al., 2003) to remove the *SA-2A-Venus* and *PGK neo* cassettes and to generate *Adam19*$^{fl/+}$ mice. Genotyping was performed by PCR using primers L1F 5′-CTGTCAGGCTCAGATAAGAAAAAGTC-3′ and F2R 5′-TGAGCA AGACTCTCACAGGTG-3′ (Figures S1A and S1C). The noon of the day when the plug was detected was considered embryonic day 0.5 (E0.5). All mice were maintained on the C57BL/6J genetic background and both genders were used. All animal housing, breeding, and experiments were performed following the guidelines of Kyoto University and RIKEN Kobe Branch, and they were approved by the Animal Research Committee of Kyoto University (Permit Number: 120170) and Institutional Animal Care and Use Committee of RIKEN Kobe Branch (Permit Number: A2001-03-73), and all efforts were made to minimize animal suffering.

Cells

HEK293T cells cultured in DMEM supplemented with 10% FBS (Moregate) were transfected with Tet-on-Adam19 or -Adam19-E347A and *pCAG-PBase* (*piggyBac* transposase) at a molar ratio of 7:1 using Lipofectamine 2000 (Thermo Fisher Scientific) according to the manufacturer's instructions. Stably transfected clones were obtained by antibiotic selection with 100 μg/ml hygromycin B (Wako) and 1 μg/ml puromycin (Sigma-Aldrich) and FACS sorting with anti-HA antibodies (Sigma-Aldrich, H3663; 1:400), anti-ALK-2 antibodies (R&D Systems, MAB637; 1:200) or anti-FLAG antibodies (Sigma-Aldrich, F1804; 1:400), and cells were analyzed in different assays (Figures 5C, 5E, and S7). For the doxycycline induction assay, cells were incubated with or without 2 μg/ml doxycycline (LKT Labs) for 24 h. For inhibition of Adam19 protease activity, cells were treated with 15 μM BB94 (Batimastat; MedChem Express) at the same time as with doxycycline. To inhibit proteasomal degradation, cells were treated with 10 μM bortezomib (LC Laboratory) for the last 6 h of the assay. In the BMP6 treatment experiment, cells were incubated with 2 μg/ml doxycycline for 36 h and with 10 μM bortezomib for the last 12 h, and then with 100 ng/ml recombinant human BMP-6 (PeproTech) for 3 h. Cultured cells were maintained at 37°C and 5% CO_2.

METHOD DETAILS

Cell Sorting

Mice at different stages of pregnancy were sacrificed by cervical dislocation and embryos were extracted. Isolated head, heart, and trunk tissues were cut into small pieces and digested with 0.2% collagenase type 2 (Worthington) by gentle pipetting. Dissociated cells were resuspended in DMEM (Thermo Fisher Scientific) supplemented with 2 mM EDTA and 5% heat-inactivated fetal bovine serum (FBS; Moregate), and filtered through 35-μm cell strainer caps (BD Falcon). tdT^{+} cells were sorted using a FACSAria II cell sorter (BD Biosciences) and considered CNCCs.

Quantitative PCR

FACS-sorted tdT$^+$ or tdT$^-$ CNCCs were directly collected into TRIzol (Invitrogen) for total RNA extraction and cDNA was synthesized using SuperScript VILO (Invitrogen) according to the manufacturer's instructions. Quantitative PCR was performed in a Step One Plus PCR System (Applied Biosystems) using Power SYBR Green PCR Master Mix (Applied Biosystems) and the following primers:

Adam19 forward 5′-CTTCCAAGGCACCACCAT-3′ and
reverse 5′-TGGCATTCTCGGAGTGGT-3′;
Rpl13a forward 5′-GTGGTCCCTGCTGCTCTCAAG-3′ and
reverse 5′-CGATAGTGCATCTTGGCCTTTT-3′.

The expression of the *Adam19* gene was normalized to that of the ribosomal protein L13a-encoding gene (*Rpl13a*) used as a control.

Microarray Analysis

To identify genes differentially expressed in *Adam19*$^{+/+}$ and *Adam19*$^{-/-}$ CNCCs, total RNA was extracted from sorted tdT$^+$ CNCCs using the RNeasy Plus Micro Kit (QIAGEN) and analyzed using Mouse Gene 1.0 ST Array (Affymetrix). The top 100 genes showing the highest expression difference were evaluated with the WAD method using R software (Kadota et al., 2008).

Histology and Immunostaining

Embryonic and fetal hearts were isolated, fixed with 4% paraformaldehyde in phosphate buffered saline (PBS) at 4°C for 2–16 h, and immersed in 30% sucrose in PBS. Fixed hearts were embedded in FSC22 compound (Leica), frozen in liquid nitrogen, and sectioned at 10-μm thickness using a cryostat (Leica). The quality of the thawed samples was verified based on the expression of Venus or GFP proteins detected by an anti-GFP antibody. Sections were washed thrice with PBS containing 0.1% Triton X-100 for 5 min and incubated with blocking solution (Blocking One, Nacalai) for 1 h at room temperature. Immunostaining was performed using the following primary antibodies: goat anti-GFP (Rockland, 600-101-215; 1:100), mouse anti-Myh1 (DSHB, MF20; 1:100), rat anti-CD31 (BD PharMingen, 550274; 1:400), rabbit anti-Sox9 (Millipore, AB5535; 1:1000), rabbit anti-aggrecan (Millipore, AB1031; 1:400), rabbit anti-Col1a1 (Bio-Rad, 2150-1410; 1:400), rabbit anti-Sm22a (Abcam, ab14106; 1:1000), rabbit anti-Col2 (Abcam, ab34712; 1:100), rabbit anti-phospho-Smad1/5/9 (Cell Signaling Technology, 13820; 1:100), and mouse anti-Alk2 (R&D systems, MAB637; 1:100). Signals were detected using secondary antibodies conjugated with Alexa488/594/647 (Molecular Probes; 1:500); nuclei were counterstained with DAPI. For whole-mount immunostaining, samples were processed according to the iDISCO protocol (https://www.idisco.info) (Renier et al., 2014) and cleared with CUBIC-1 reagent (Susaki et al., 2014). All images and movies were acquired using a TCS-SP8 confocal microscope system and the LAS X software (Leica).

Quantification of Cell Apoptosis and Proliferation

The TUNEL assay was performed using the ApopTag® Plus *In Situ* Apoptosis Fluorescein Detection Kit (Millipore, S7111) according to the manufacturer's instructions. Subsequently, sections were immunostained for Ki67 (Abcam, ab15580; 1:1,000) and counterstained with DAPI. The ratios of apoptotic to total nuclei and proliferative to total nuclei in CNCC clusters were quantified using the Volocity software (PerkinElmer).

Cartilage Staining

For whole-mount heart staining, excised hearts were first fixed in 4% paraformaldehyde in PBS at 4°C for 16 h and then in 95% ethanol for 16 h and acetone for 16 h and stained with 0.03% alcian blue 8GX (MP Biomedicals) in 70% ethanol at 37°C for 2 days. Hearts were incubated in 1% potassium hydroxide until complete discoloration, dehydrated in methanol series (50%, 75%, and 100%) in PBS for 20 min and cleared in benzyl benzoate:benzyl alcohol (2:1) for 1 h. Images were captured using an M205C stereomicroscope (Leica). Cryosections were stained with 0.1% alcian blue 8GX in 3% acetic acid for 30 min at room temperature, washed three times with 3% acetic acid and 0.1% Triton X-100 in PBS, and immunostained with antibodies. After observation under a TCS-SP8 confocal microscope, sections were rinsed in 0.1% Triton X-100/PBS and counterstained with eosin. Images were captured under a BX50 microscope (Olympus) equipped with a DP72 digital camera (Olympus) and the size of alcian blue-positive cartilage was measured using the DP2-BSW software (Olympus).

Plasmids

Expression plasmids for mouse type I Bmp receptors (Bmpr1a/Bmpr1b/Alk2) and human ALK2 containing a C-terminal Myc tag were purchased from Sino Biological Inc. Mouse *Bmpr2* was subcloned into the pCMV3-C-Myc mammalian expression vector (Sino Biological Inc). In some experiments (Figures 5C and S7), an HA or 3xFLAG tag was introduced directly after the signal sequence in all Bmp receptor expression plasmids. The Tet-on vector used in this study was based on PB-TAC-ERP2 (Kim et al., 2016), where the main expression cassettes were flanked by inverted *piggyBac* terminal repeats enabling their stable genome integration (Figure 5B). Human *ADAM19* cDNA was purchased from Sino Biological Inc. Mouse *Adam19* or human *ADAM19* was subcloned into the pDONR vector (Thermo Fisher Scientific) and then introduced into the PB-TAC-ERP2 Tet-on vector using the Gateway system

(Thermo Fisher Scientific). Mutant mouse *Adam19* and human *ADAM19* genes encoding the EA substitution in the Adam19 catalytic site were obtained by PCR as previously described (Chesneau et al., 2003) using the following primers:

mouse *Adam19* E347A forward 5′-GCGATTGGCCACAACTTTG-3′ and reverse 5′-ATGGGCCACAGTGGAGGCTA-3′;
human *ADAM19* E346A forward 5′-GCGATGGGCCACAACTTT-3′ and reverse 5′-GTGGGCCATGGTGGCAG-3′.

Western Blotting Analysis

HEK293T cells were lysed in RIPA buffer (10 mM Tris-HCl, pH 7.4, 150 mM NaCl, 1 mM EDTA, 0.1% SDS, 1% NP-40, 0.1% sodium deoxycholate) containing 1% protease inhibitor cocktail (Nacalai) with magnetic stirring at 4°C for 1 h and subjected to SDS-PAGE. Proteins were transferred onto PVDF membranes (Immobilon-P; Millipore) and probed with the following primary antibodies: mouse anti-Myc tag (Cell Signaling Technology, 2276S, 9B11; 1:2,000), rabbit anti-Adam19 (generated in the Sehara lab; 1:2,000), mouse anti-β-actin (Santa Cruz, sc-69879, clone AC-15; 1:2,000), mouse anti-HA (Sigma-Aldrich, H3663; 1:2,000), rabbit anti-phospho-Smad1/5/9 (Cell Signaling Technology, 13820; 1:400), and anti-Smad1 (Cell Signaling Technology, 6944, D59D7; 1:2,000). After washing, protein-primary antibody binding was detected with HRP-conjugated anti-mouse or anti-rabbit IgG (Cell Signaling Technology; 1:5,000) and visualized by chemiluminescence (ECL Plus; GE Healthcare). Images were acquired with ImageQuant LAS 4000 (GE Healthcare).

LDN-193189 Treatment

Mice were treated with LDN-193189, a BMP type I receptor inhibitor, as previously described (Yu et al., 2008) with minor modifications. Briefly, LDN-193189 (Sigma-Aldrich) was dissolved in 10% dimethyl sulfoxide (DMSO) in PBS and administered to pregnant mice intraperitoneally (3 mg/kg every 12 h) at E14.25–E16.25; 10% DMSO in PBS was administered to the control group. The treated embryos were analyzed at E18.5 (Figure 6A).

QUANTIFICATION AND STATISTICAL ANALYSIS

All statistical analyses were conducted using R statistical software (v3.1.2). The significance of the differences between two groups was analyzed by Student's t test and among more than two groups by one-way analysis of variance (ANOVA) followed by Tukey's post hoc test. The LDN-193189 treatment data (Figure 6C) were analyzed using two-way ANOVA followed by Tukey's post hoc test. *P*-values less than 0.05 indicated statistical significance.

DATA AND CODE AVAILABILITY

The accession number for the array data reported in this paper is Gene Expression Omnibus: GSE99551.